




Matthew Siegler¹ , Paul Warren² , Katelyn Lehman Franco^{1,3}, David Paige², Jianqing Feng¹ , and Mackenzie White^{1,3}

¹Planetary Science Institute, Tucson, AZ, USA, ²University of California, Los Angeles, Los Angeles, CA, USA, ³Southern Methodist University, Dallas, TX, USA

Key Points:

- We produce a self-consistent forward model of lunar surface heat flux
- This models can provide a basis for future, targeted heat flux measurements
- We provide a best fit lunar bulk, crustal, and mantle radiogenic element composition consistent with present day data

Correspondence to:

M. Siegler,
msiegler@psi.edu

Citation:

Siegler, M., Warren, P., Franco, K. L., Paige, D., Feng, J., & White, M. (2022). Lunar heat flow: Global predictions and reduced heat flux. *Journal of Geophysical Research: Planets*, 127, e2022JE007182. <https://doi.org/10.1029/2022JE007182>

Received 10 JAN 2022

Accepted 20 JUL 2022

Author Contributions:

Conceptualization: Matthew Siegler, Paul Warren, Katelyn Lehman Franco, David Paige
Formal analysis: Matthew Siegler, Paul Warren, Katelyn Lehman Franco, Jianqing Feng
Funding acquisition: Matthew Siegler, David Paige
Investigation: Mackenzie White
Methodology: Matthew Siegler, Katelyn Lehman Franco, Jianqing Feng
Project Administration: Matthew Siegler
Resources: Paul Warren
Software: Matthew Siegler
Supervision: Matthew Siegler
Visualization: Matthew Siegler
Writing – original draft: Matthew Siegler, Paul Warren, Katelyn Lehman Franco
Writing – review & editing: Matthew Siegler, Katelyn Lehman Franco, Mackenzie White

Abstract Geothermal heat flux of a body provides a unique look into its internal composition. The geothermal heat flux of the Moon is believed to vary primarily due to the distribution of radiogenic materials both spatially and vertically through the lunar crust. Here, we combine available global orbital, landed mission, returned sample, and meteorite data to produce a forward model of lunar heat flux consistent with present data. This provides a framework for future geothermal and geochemical measurements over the lunar surface, which can be tied back to global radiogenic and refractory element composition. We develop a model of the Moon as a single heat flux province represented by ~60% of the Lunar Prospector Gamma-Ray Spectrometer surface Th value or equivalently a 21.5 km thick layer with surface Th values. The zero-thorium intercept, or “reduced heat flux,” of these models is approximately 5 m Wm⁻², implying the net heat flux from the mantle is at or below this value. With an estimated Urey ratio between 0.65 and 0.73, this equates to a mantle thorium concentration of ~19–~25 ppb. This model suggests a bulk thorium concentration of approximately 50.5 ± 5.5 ppb. This value is based on the heat flux that would be obtained from a $C_{Th}/C_U = 3.7$, $C_K/C_U = 2,000$ = or equivalently 13.7 ± 1.5 ppb of uranium and 27.2 ± 3.0 ppm potassium.

Plain Language Summary The heat flowing out of the lunar interior provides a window into the composition and temperatures of the lunar interior. Most of this heat is produced by radioactive elements in the crust (uranium, thorium, etc.). Across the Moon, both the crustal thickness and concentration of radioactive elements can change dramatically. Crustal thickness was measured in detail by the GRAIL (~2012) and surface radioactive element concentration by Lunar Prospector (1999) missions. Both crustal thickness and radioactive elements were found to change regionally, with the near side region known as Procellarum being a major oddball with very thin crust and high concentrations of radioactive rocks. Here, we make models to predict how the heat flux of the Moon will vary from place to place to match both Apollo era and future heat flux measurements. The few measurements we have provide a biased view of what the Moon and a whole is made of. These models will aid in deciding where to land future lunar missions measuring heat flux or returning samples to best constrain the composition of the entire Moon.

1. Introduction

Geothermal heat flow is a fundamental measure of a planet's internal composition and evolution. The Moon is not strongly tidally heated, has lost its heat of formation, and is not likely to have strong mantle convection. Therefore, the surface heat flux of the Moon results predominantly from the subsurface column abundance of radiogenic material (e.g., U, Th, and K). Since U, Th, and K are concentrated in the lunar crust due to their lithophile nature, most of the heat flux seen at the surface is expected to be a crustal source. Therefore, a characterization of this crustal variation is needed to examine the underlying bulk mantle composition and to calculate the heat budget of the Moon as a whole.

The radiogenic and incompatible elements (namely Th and U) have large ionic radii and high ionic charges, causing these two elements to partition into the melt preferentially. Therefore, Th and U are exceptionally useful for constraining the Moon's history of differentiation. Based on the differentiation process of a lunar magma ocean, the ferroan anorthosite (FAN) lunar crust would have low U and Th concentrations, leaving higher U and Th concentrations in a sub-crustal melt which may have migrated, at least in part, to the Procellarum region. Radiogenic concentrations in the FAN may increase with depth due to the low partition coefficients of U and Th in plagioclase (Sun et al., 2017), and the increasing concentration of the incompatible elements in the residual melt (e.g., Moriarty et al., 2020; Warren & Wasson, 1979) or may decrease with depth (Warren, 2001) if much of the

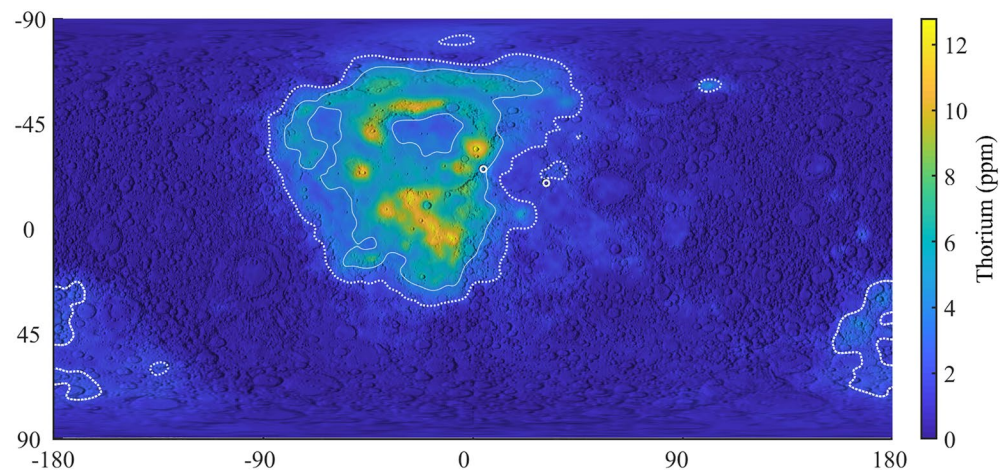


Figure 1. Thorium Map (ppm) based on Lunar Prospector Data (Lawrence et al., 2003; rescaled to Warren, 2005 as described below)—Note the strong asymmetry centered on the nearside Procellarum KREEP Terrain and farside South Pole-Atkin regions. White dashed lines mark 2 ppm Th, solid lines 4 ppm Th. White circles mark the Apollo 15 and 17 sites.

immiscible material somehow migrated to the nearside. Therefore, surface heat flux measurements could provide unique characterization of the composition of the crust as a function of depth.

These radiogenic elements are also helpful for constraining the overall composition of a planetary body because they are both refractory and lithophile. Among primitive Solar System materials, the refractory lithophile elements behave as a coherent group. Thus, knowledge of one helps to constrain the other members in the group, including, Be, Sc, Ti, V, Sr, Y, Zr, Nb, Ba, the 14 rare-earth elements, Hf, Ta, and the major oxides Al_2O_3 and CaO. The concentrations of 10 additional incompatible elements (Li, B, Na, K, Br, Rb, I, Cs, Mo, and W) can be correlated with relative Th concentrations. Major rock-forming elements Si and Mg are also considered refractory.

Quantifying the total heat-producing elements content of the lunar crust requires heat flux characterization of the crust as a whole, which may vary spatially in both radiogenic concentration and thickness. Fitting multiple heat flux measurements can elucidate the depth distribution of radiogenic elements, which can also constrain general crustal composition as a function of depth (e.g., Stein, 1995). Broadly distributed measurements will also offer a constraint on the reduced heat flux (essentially the crust-free heat flux), which will allow for a separation of the mantle heat production component. Part of this mantle component is from the slow release of past heat, also mainly from radiogenic sources in the case of the Moon. This current versus past heat loss is characterized by a value known as the Urey ratio (the ratio between total heat loss and present-day heat production). The Urey ratio provides a constraint on the presence of convection Laneuville et al., (2013, 2018) and the efficiency of planetary cooling.

While the Moon does not have areas of anomalously high heat flux (such as mid-ocean ridges) due to a lack of plate tectonics, the Moon is known to have a highly asymmetric surface composition (e.g., Lawrence et al., 2003) and crustal thickness (Wieczorek et al., 2013). This surface characteristic likely results from interior asymmetries (Laneuville et al., 2013; Wieczorek & Phillips, 2000) and causes a spatially varying surface heat flux (both past and present). Our understanding of the thermal evolution and composition of the bulk moon therefore needs to capture a global picture of the present lunar thermal state.

Unfortunately, the constraints of surface heat flux from the Apollo 15 and 17 Heat Flow Experiments (HFE) likely do not reflect the Moon as a whole (e.g., Siegler & Smrekar, 2014; Warren & Rasmussen, 1987). Surface heat flux values at these sites are 21 ± 3 and 14 ± 2 m W m^{-2} , respectively (Langseth et al., 1976; Warren & Rasmussen, 1987), well elevated over the expected lunar background (Wieczorek & Phillips, 2000). The location of the HFE sites was near the edge of an area now known as the Procellarum KREEP Terrain (PKT, with KREEP standing for potassium, rare earth elements, and phosphorus) and was first identified by an anomalously high crustal thorium concentration (Haskin et al., 2000; Jolliff et al., 2000; Lawrence et al., 2000), seen in Figure 1. These maps are rescaled following Warren (2005) as detailed in the following section. Roughly coincident with the lunar nearside Mare, this region may have been the center of an anomalous thermal structure (Wieczorek &

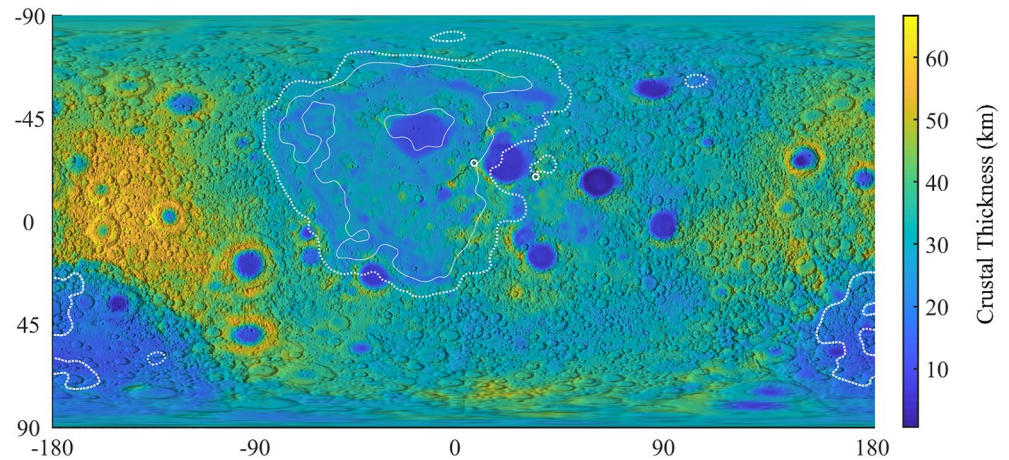


Figure 2. Global Crustal Thickness (km) based on Gravity Recovery and Interior Laboratory data (Wieczorek et al., 2013, Model 4). White dashed lines mark 2 ppm Th, solid lines 4 ppm Th. White circles mark the Apollo 15 and 17 sites.

Phillips, 2000). Evidence suggests that this mantle scale thermal asymmetry still exists today (Grimm, 2013; Laneuville et al., 2013; Siegler et al., 2016).

Future surface heat flux and seismic observations will be affected by a mantle thermal anomaly, so the placement of geophysical instruments both inside and outside of this region is critically important for understanding the lunar interior. The unfortunate coincidence that Apollo geophysical measurements lie areas within or directly abutting the PKT highlights the importance of location for in situ geophysical study. Here, we attempt to combine our current state of knowledge of lunar composition and geophysics to deliver global predictions of the surface heat flux of the Moon. We will identify areas with the highest uncertainty to provide insight into the placement of future landed geophysical missions.

2. Recent Advances and New Data in Crustal Thickness and Compositional Constraints

Recent missions, such as the Gravity Recovery and Interior Laboratory (GRAIL) and Lunar Reconnaissance Orbiter (LRO), have significantly impacted our knowledge of the lunar geophysical state. GRAIL's formation of flying spacecraft allowed for an unprecedented characterization of the lunar gravity field (Zuber et al., 2012). This new data has allowed for the inversion of crustal thickness, density, and density gradient (Andrews-Hanna et al., 2013; Besserer et al., 2014; Wieczorek et al., 2013). Here, we focus primarily on crustal thickness and assume a constant crustal and mantle density-however, our fit heat production with depth could be interpreted as at least in part due to changes in bulk density. New topography data have come from the LRO, Lunar Orbiting Laser Altimeter (LOLA), LRO Camera (LROC), and Selene Terrain Camera (TC) (e.g., Scholten et al., 2012). In addition, the LRO Diviner Lunar Radiometer Experiment (DLRE) provides measurements of global surface temperatures of the Moon (e.g., Williams et al., 2017).

Wieczorek et al. (2013) developed several crustal thickness and density models with average crustal thickness values between 34 and 43 km. These models predict between 29.0 and 38.0 km thick crust at the Apollo 12 and 14 landing sites, which fit within the constraints set by Apollo (Gagnepain-Beyneix et al., 2006; Lognonné et al., 2003). Figure 2 shows the crustal thickness for Wieczorek et al.'s (2013) Model 4, with 43 km average thickness. Much of the model variation comes from a trade between assumed crustal and mantle densities. The average density of the highlands crust in these models was $2,550 \pm 250 \text{ kg m}^{-3}$, which we adopt here. The following section will address the variations these models predict on surface heat flux and highlight areas where in situ heat flux observations will provide the most effective constraint in differentiating these models.

LRO and other recent spacecraft have added details to our understanding of composition and near-surface radiogenic element abundance, but the most global mapping of elemental compositional data comes from the 1998 Lunar Prospector mission Gamma-Ray Spectrometer (Feldman et al., 1999; Lawrence et al., 2003). This

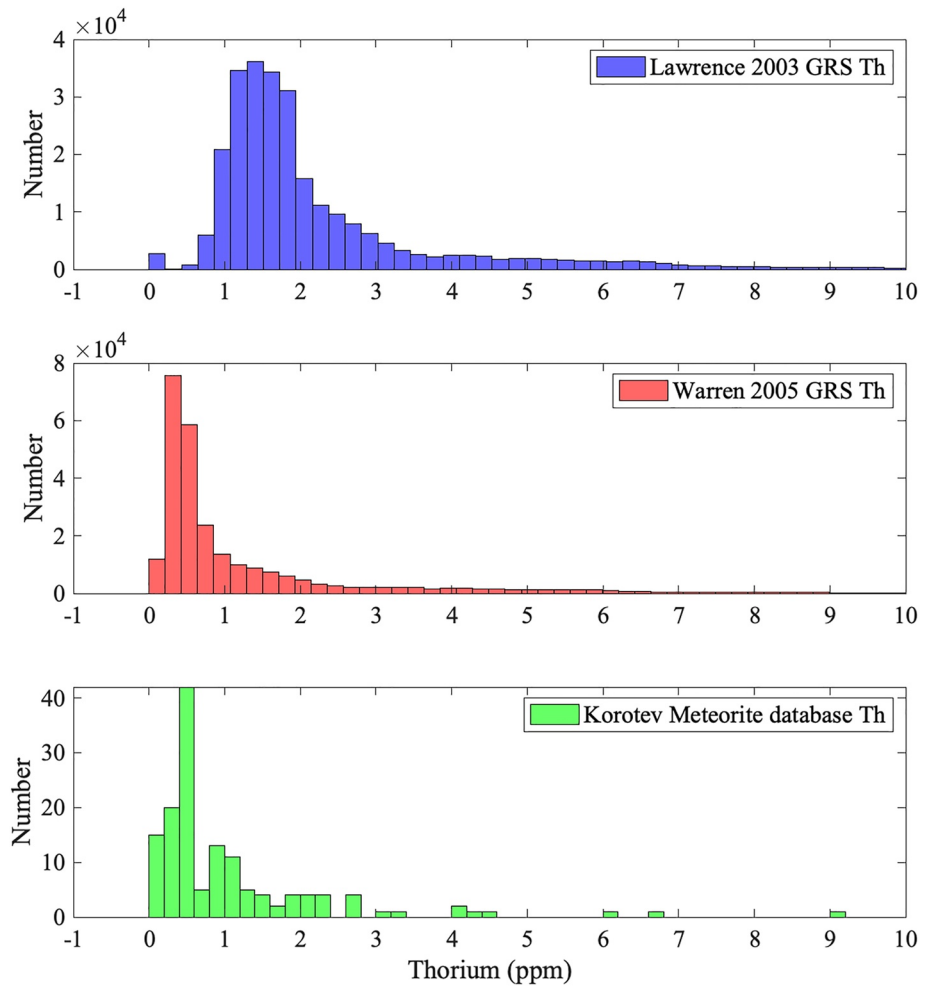


Figure 3. Global Thorium as determined from Lawrence et al., 2003 and our adopted recalibration from Warren (2005), updated here with samples compiled by Korotev (2012, 2017) as compared to Th distribution in the lunar meteorite collection. Number means number of $\frac{1}{4}$ degree GRS “pixels” for the upper plots and number of samples for the lower plot falling in a given Th concentration bin.

mission’s low orbit (30–40 km) allowed for mapping radiogenic material (e.g., thorium) in the near-surface with a resolution that has yet to be surpassed. However, the initial calibration of this data (e.g., Lawrence et al., 2003) relied on the Apollo sample suite dominated by KREEP-rich samples.

The absolute calibration of the Gamma-Ray Spectrometer results has been revised here following Warren (2005), which recalibrated the data set to lunar meteorite compositions to represent a more global sampling distribution (Paige et al., 2016). As Figure 3 illustrates, this recalibration of the Lunar Prospector Gamma-Ray Spectrometer (LP-GRS) data is more representative of the global sample distribution of Th. As discussed by Gillis et al. (2004) and Warren (2005), comparison with samples including lunar meteorites reveals how difficult it is to calibrate the GRS data for low-Th regions. Meteorite data here are compiled from Korotev (2012, 2017), Korotev and Zeigler (2014), and Korotev and Irving (2021). The global average surface Th results have ranged from 1.2 (Gillis et al., 2004) to 2.4 ppm (Lawrence et al., 2000). The orbital GRS results we cite here are based on averaging the calibrations of Lawrence et al. (2003), Warren (2005), Prettyman et al. (2006), Yamashita et al. (2010), and Zuo et al. (2014). The average global surface Th using these five data sets is 1.49 ppm.

Somewhat unfortunately, both the Apollo 15 and Apollo 17 heat flux measurements are situated just to the mare side of a mare/highland boundary (Langseth et al., 1976). However, one can assume that the heat flow in both locations is far more closely linked to the composition of the local highland crust than to the relatively thin local mare-surface composition. In general, the maria are only thin veneers, generally less than 2 km thick, over the

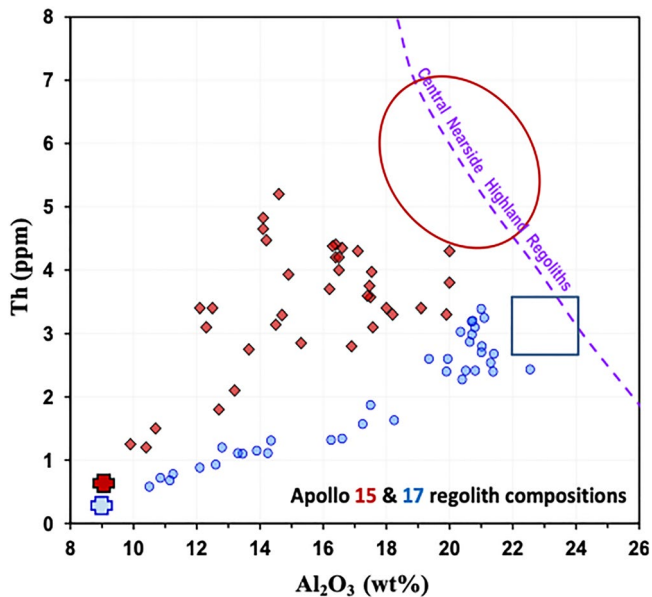


Figure 4. At mare-rim locales such as the Apollo 15 and Apollo 17 sites, thorium correlates with the highlands-linked major oxide Al_2O_3 . We extrapolate the average composition of the local highland component by assuming the Al_2O_3 wt% based on the linear relationship between Al_2O_3 - TiO_2 for the Apollo 17 regolith samples (Figure 5) or in the case of Apollo 15 (less precisely) by a generic trend of Th- Al_2O_3 anticorrelation among central nearside pure highland regoliths (Warren & Kallemeyn, 1991). Cross symbols indicate mean compositions of preponderant types of local mare basalts. Data sources include Keith et al. (1974), Waenke et al. (1974, 1975), Laul et al. (1974), Rose et al. (1974), Rhodes et al. (1974), and especially Korotev (1987) and Korotev and Kremser (1992).

older highland crust (Gong et al., 2016; Thomson et al., 2009). We discuss the specific circumstances of the two Apollo sites below.

Apollo 15: The Apollo 15 site at 26.1341°N, 3.6299°E (Wagner et al., 2014, LPSC) is on a fringe of Mare Imbrium where the mare fill appears to be well under 500 m thick (Thomson et al., 2009). The overall crustal thickness at this locale is ~ 29 – 40 km (Taylor & Wiczorek, 2014), who chose one of the thinnest among the crustal-thickness calibrations discussed by Wiczorek et al. (2013). Thus, probably 98%–99% of the subjacent crust is of non-mare, “highland” affinity, and only 1%–2% is mare. This area was best fit by a 21 ± 3 m Wm^{-2} heat flux by Langseth et al. (1976).

Both orbital-GRS and sample data constrain the composition of the local highland crust. The orbital Th data indicate an average Th concentration of ~ 5.1 ppm, but with an uncertainty that is admittedly hard to gauge (because both the nominal results and the calibrations are uncertain; see above); we somewhat arbitrarily estimate a 2- σ uncertainty of 1.5 ppm. Evidence from Apollo 15 samples does not constrain the regional-average Th as tightly as we might wish.

There is a rough correlation between Th and the major oxide Al_2O_3 (Figure 4). The data fan out from the well-known and very Th-poor composition of the local mare basalts toward a diverse mix of more Al- and Th-rich highland regolith with KREEP, mare, and FAN materials. The average composition of the highland end-members likely falls near the dashed curve in Figure 4, derived from an overall anticorrelation between Al_2O_3 and Th (and other incompatible trace elements) among all known lunar pure-highland regoliths (e.g., Warren & Kallemeyn, 1991). Thus, the Apollo 15 sample trend extrapolates to an average regional highland composition of 20.5 wt% Al_2O_3 and 5.7 ± 1.3 ppm Th. Averaging this with the orbital GRS result, which samples a larger area (which includes both highlands and mare), we arrive at $5.5 \pm (2-\sigma) 1.0$ ppm Th as our final estimate for the relevant composition for this heat flow measurement site.

This Apollo 15 thorium estimate is significantly higher than the values assumed in some previous heat-flow interpretations, which seem to have relied almost entirely on orbital GRS. Langseth et al. (1976) assumed 3.8 ± 0.7 ppm. Yoshida et al. (2001) assumed 3.6 ± 0.2 ppm. Zhang et al. (2014) assumed 5.05 (\pm “less than” 0.5) ppm.

Apollo 17: The Apollo 17 site at 20.1923°N, 30.7655°E (Wagner et al., 2014), is on a fringe of Mare Serenitatis where massifs of highland material surround an 8-km wide mare valley. Despite being marginal to Serenitatis, the mare fill here is likely relatively thick, possibly reaching 3 km (Grimm, 2018). Still, the overall crustal thickness at this locale is ~ 31 – 41 km (Taylor & Wiczorek, 2014), and the proximity of Th-rich highland regolith both north and south of the site suggests that for heat flow, the effective thickness of the mare fill is less than the local maximum value. Depending upon the shape of the mare-bottom (roundish or squarish), lateral diffusion of heat into the low-porosity (and therefore higher-conductivity) mare fill may enhance the local heat flow above its predicted value in the absence of the mare (Sieglar & Smrekar, 2014; Warren & Rasmussen, 1987). We assume this effect approximately offsets the lower Th content of the minor mare portion of the crust. Thus, the local highland Th content effectively determines the local crust-sourced heat flow. This area was best fit by a 14 ± 2 m Wm^{-2} heat flux (Langseth et al., 1976; Warren & Rasmussen, 1987).

Orbital Th constraints from this site are challenging to interpret and ultimately highly uncertain because the orbital GRS technique has limited spatial resolution (not significantly improved from the data acquisition orbital altitude [~ 40 km at the lowest orbit]). Additionally, the boundary between mare and highland in this region is notably complex. The 50 km to the northeast and east of the site is dominantly a highland surface. Still, this region probably has important, scattered (impossible to resolve using orbital GRS) areas of outlying mare materials. Taken

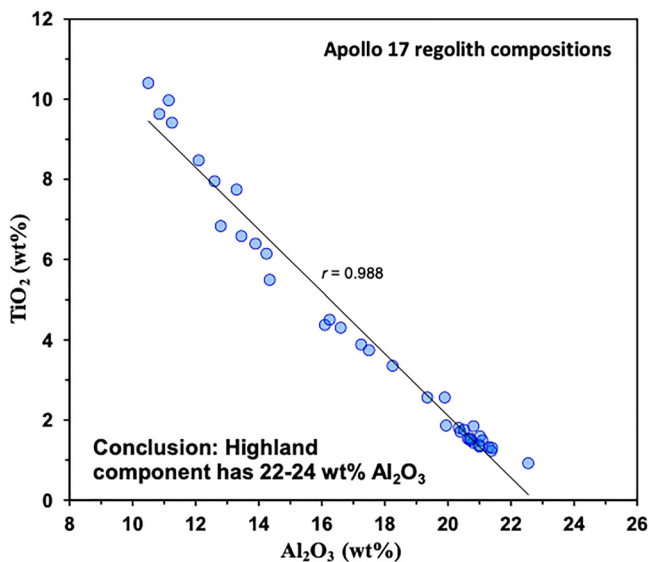


Figure 5. Apollo 17 regolith compositions show an anticorrelation between TiO₂ and the highlands-linked major oxide Al₂O₃. We constrain the average local highland composition to have 22–24 wt% Al₂O₃ based on extrapolation of this trend to roughly 0.2 wt% TiO₂. Data sources include Keith et al. (1974), Waenke et al. (1974, 1975), Laul et al. (1974), Rose et al. (1974), Rhodes et al. (1974), and especially Korotev and Kremser (1992).

at face value, the orbital GRS data (same sources as for Apollo 15) suggest, with significant scatter, that the regional highland regolith Th concentration is roughly 2 ppm. But this is best interpreted as a lower limit.

Fortunately, evidence from Apollo 17 samples appears to constrain the regional-average Th concentrations of the highland regolith rather well. There is a tight correlation between Th and the major oxide Al₂O₃ (Figure 4). While TiO₂ is very high in the mare basalts (Figure 5), the FAN-dominated highland regolith component has a low TiO₂ concentration. Based on the correlation between Th and Al₂O₃ the highland FAN component would have approximately 23 wt% Al₂O₃. The trend in Figure 4 extrapolates to intercept that Al₂O₃ at 2.7–3.6 ppm Th. By taking the weighted average of this result with the mare-biased orbital GRS result, we arrive at $3.1 \pm (2-\sigma) 0.5$ ppm Th as the appropriate highland composition for this heat flow measurement site.

3. Initial Global Model Results

In making a forward model of surface heat flux, we should briefly compare the rather simplistic approach taken here to methods used in previous papers such as Taylor and Wieczorek (2014), Laneuville et al. (2013, 2018), and Siegler and Smrekar (2014). Generally, these models test some assumption of underlying, unseen heat producing elements. Most notably, following Wieczorek and Phillips (2000), test the existence of a KREEP-rich layer under or mixed within the lunar crust. Taylor and Wieczorek (2014) further models different assumed crustal column composition in differing regions. This requires some assumption of how modeled subsurface material is distributed.

In the simplified approach in this paper, we assume spatial distribution of subsurface materials mirrors surface concentrations exactly. We do not take into account potential subsurface KREEP, measurable basin ejecta blanket or mare thickness, lateral heat flow, or models of internal mantle convection as discussed extensively in these other works. In that sense, this is meant to be a baseline model consistent with direct observations from which inferred subsurface changes can be added if future measurements demand them.

The direct observations we use are the crustal thickness and density described by GRAIL (Wieczorek et al., 2013) and our recalibrated LP-GRS based Th values (Lawrence et al., 2003; Warren, 2005). With these, we can now build a simple heat production model varying assumed radiogenic distribution within the crustal column. As noted with the Apollo sites, local mare infilling, ejecta blankets, etc., can modify the actual crustal Th from this GRS-derived value on the scale of comparing to Apollo samples. Local areas may contain higher Th at scales below the LP-GRS resolution, such as the ~25 km Compton-Belkovich volcanic complex (Wilson et al., 2015). Therefore, global GRS-based models will likely provide a slight underprediction in heat flux, but can provide a base model to compare future lunar measurements at specific locations and type localities.

To determine the heat flux, we need to be able to effectively estimate Th concentrations with depth. The upper ~10 km of the crust is considered to be a part of the mega-regolith with the upper portion of the regolith representing variable mixtures of materials from the mare, Mg-suite, anorthositic highlands, and KREEP terrain formed from global mixing during impacts. In the low-Th Feldspathic Highlands Terrain, evidence points to an increase in plagioclase with depth as you get to more of undisturbed crust. This change can be represented by a near-surface pyroxene-rich layer transitioning to the primitive highland crust predominantly composed of low-Th, plagioclase-rich, and FAN (e.g., Martinot et al., 2018; Laneuville et al., 2018). Thorium partitions into pyroxene more readily than plagioclase with a partition coefficient of partition coefficient (0.83 for pyroxene and 0.13 for plagioclase 0.13 Dygert et al., 2017), suggesting that the pyroxene layer would have a higher Th content.

Warren (2001) compared large crater (>60 km) GRS-based Th concentrations to their ejecta, concluding deeper crustal materials should decrease the column thorium average abundance to ~30%–76% that of the surface, implying concentrations of ~0.98 ppm for the average crustal column abundance. Studies of Apollo 16 samples suggest that the deeper feldspathic highlands crust may be much poorer in Th than the surface, with Th concentrations averaging 0.05 ± 0.03 ppm from three anorthite samples from Apollo 16 (Laneuville et al., 2018; Meyer, 2005).

As a reference, the primitive Earth mantle is ~ 0.08 ppm Th (McDonough & Sun, 1995). Therefore, we will also apply this 0.05 ppm lower, feldspathic crustal Th concentration in our first-order models.

In part to avoid prescribing a “shallow Th” versus “deep Th” model, we use a one-dimensional thermal conduction model in this work, differing from earlier publications by our group. A 1D approach allows for the enhanced radiogenic material to be at any depth in the crust and provide the same result. A 3D model will produce different results if the heat production is near surface versus at depth. Furthermore, the simplified global models here use $\frac{1}{4}$ a uniform degree spatial resolution, a 3D model would require changing grid resolution with depth (a spherical thermal model rather than a planar model), which was also a complication beyond the scope of this paper. The low spatial resolution also would result in many of the attributes of a 3D model (such as focusing of heat at crustal thickness boundaries Sieglar & Smrekar, 2014; Warren & Rasmussen, 1987) and the aforementioned depth of Th placement to be muted. A full 3D model would require much higher spatial resolution to show variations. These neglected small length-scale effects are potential errors in our best fit models to the Apollo sites, but will not greatly effect predicted global trends.

The lower crust of the lunar highlands, based on central peaks, has been argued to be noritic to gabbro-noritic in composition with 18%–25% Al_2O_3 (Lemelin et al., 2015; Spudis & Davis, 1986; Wieczorek & Zuber, 2001) or consistent with the Mg-suite rocks with variable amounts of a KREEP component and 3%–31% Al_2O_3 (Cahill et al., 2009). Cahill et al. (2009) also showed through comparing central peak speak compositions with samples that the amount of plagioclase in the lower crust was linked to the thickness of the crust with more mafic compositions below thinner crust and more plagioclase-rich compositions below the thicker feldspathic highlands crust. Despite these differences, the Mg-Suite samples still effectively modeled the lower crust and likely represents plutons emplaced at crust-mantle boundary. This is consistent with geobarometry studies of some of the Mg-suite samples which suggest a lower crustal emplacement (42–50 km for sample 76,535) (McCallum & Schwartz, 2001; Shearer et al., 2015). If the lower crust is represented by the Mg-suite, then the Th concentrations are highly variable with the KREEP-rich magnesian rocks formed within the PKT and KREEP-poor Mg-suite rocks represented by magnesian meteorites from outside the FHT (Gross et al., 2020).

As mentioned, the Procellarum region (and lesser so South Pole Aitken basin) has anomalously high radiogenic element abundances. Several studies have related localized surface concentrations to impact ejecta from a Th-rich target. The most notable is the increase in Th around the Imbrium impact basin (Hagermann & Tanaka, 2006; Haskin, 1998; Sieglar & Smrekar, 2014). Therefore, the general increase in Th in much of the Procellarum region may represent Imbrium, signaling an impact into a KREEP-rich subcrustal layer. The Procellarum region as a whole has been postulated to have been underlain by a KREEP-rich layer based on the existence of mare volcanism (Wieczorek & Phillips, 2000). However, its current (if still existing) and past extent are unknown.

Intriguing recent advances pointing toward the existence of a sub-crustal KREEP rich layer come from GRAIL gravity gradients (Andrews-Hanna et al., 2013, 2014), crustal magnetization (Wieczorek, 2018), evidence for regional uplift (Sieglar et al., 2016), electrical conductivity (Grimm, 2013), and thermal modeling (Laneuville et al., 2013, 2018). These studies highlight areas of the Procellarum region that appear to have heated dramatically in the past in a way that is not consistent with surface radiogenic element abundances alone, but instead requires at least a past, if not present-day sub-crustal KREEP-rich layer. Several studies have examined the impact a sub-crustal KREEP layer might have on the surface heat flux (Laneuville et al., 2013, 2018; Sieglar & Smrekar, 2014; Wieczorek & Phillips, 2000), with the primary question as to whether a subsurface KREEP layer is needed to explain the Apollo Heatflow Experiment results (Langseth et al., 1976).

Here, we first approach the issue of matching surface heat flux with a direct scaling of observed surface radiogenic element concentration overlying a low Th feldspathic layer (0.05 ppm Th) (Laneuville et al., 2018; Meyer, 2005). While this model may miss the heating effects from a postulated sub-crustal KREEP-rich zone or the lower crust, it offers a definable baseline model. Surface heat flux values can help constrain the proper ratio of surface to deeper crustal/mantle radiogenic concentrations and thus the bulk heat-producing element content of the Moon. For simplicity, we will assume the mantle is uniform in composition and heat flux and all spatial variation comes from crustal radiogenic elements. As noted earlier, an extensive body of work (Grimm, 2013; Laneuville et al., 2013, 2018; Sieglar & Smrekar, 2014; Sieglar et al., 2016; Wieczorek & Phillips, 2000) has looked at the effects on mantle heating from a spatially varying lower crustal KREEP-rich layer. These models were consistent generally with either a thin (<5 km) layer of KREEP-rich material at the crust-mantle interface

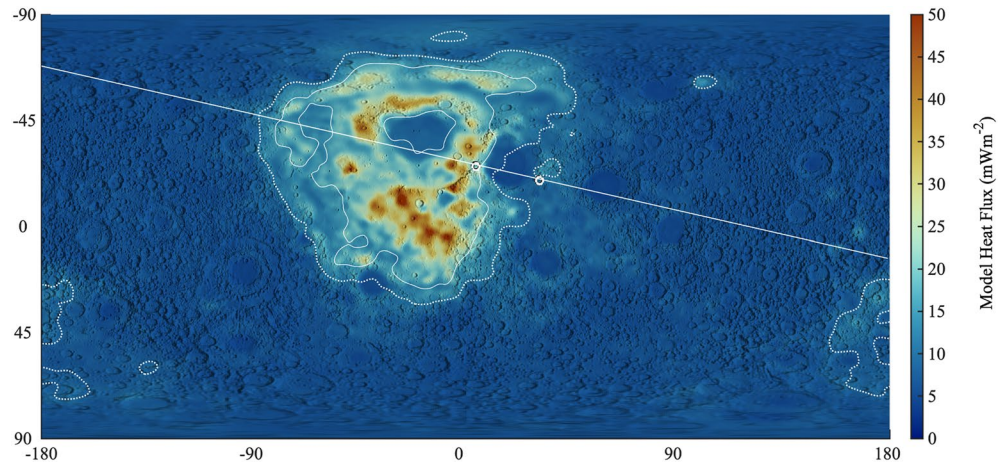


Figure 6. Model with full Lunar Prospector Gamma-Ray Spectrometer (LP-GRS) crustal heat flow assuming “model #4” crustal thickness from Wieczorek et al. (2013), 4 m W m^{-2} mantle flux, and an entire column abundance equal to that measured by LP-GRS. The straight, white line shows a transect through the Apollo 15 and 17 sites (and coincidentally the upcoming LISTER Crisium 2023 heat flow measurement) used in Siegler and Smrekar (2014) and Figures 7 and 9.

or a KREEP enrichment within the crust in the Procellarum region. Here, we will approach the existence of this enrichment generally as an enhancement within the crust and treat it as directly proportionate to the concentrations of radiogenic material seen at the lunar surface. We will briefly discuss enhancements that we expect given a lower crustal heat-producing layer spatially distinct from the surface Th anomaly. Still, the two Apollo heat flow locations are insufficient to add much detail to the potential shape of this KREEP-rich body. Such a body has generally been treated as around 1,500–1,800 km disc (e.g., Siegler & Smrekar, 2014), but if present likely has a spatial distribution more closely following observed gravity (Andrews-Hanna et al., 2014) or magnetic (Wieczorek, 2018) anomalies.

The simplest case is to assume that the surface Th is directly representative of the entire column to begin our model approach. This “high heat flux” endmember is shown in Figure 6, with model details discussed below. We assume that the weight ratio U and K (C_K/C_U) is constant at 2,000. Conveniently, the ratio Th/U is essentially constant, 3.7 by weight, in lunar materials. This consistency arises because of their large ionic radii. Among lunar materials, K/U shows far more scatter than Th/U (Warren, 2005). However, the uncertainty of roughly 20% in average K/U is almost negligibly small because U, Th, and K, at the assumed ratios, contribute to current heat production in proportions of 48.3%, 48.2%, and 3.5%, respectively. The current heat-generation rate (Jaupart & Mareschal, 2014) for this compositional relationship amounts to 53.1 W per kilogram of Th (with associated U + K).

Using the $C_{Th}/C_U = 3.7$ and $C_K/C_U = 2,000$ concentration ratios, we use the standard relationship (Jaupart & Mareschal, 2014) where heat production per unit mass, H (W kg^{-1}), is found by:

$$H = 0.9927 C_U \times H^{238\text{U}} + 0.0072 C_U \times H^{235\text{U}} + C_{Th} \times H_{Th} + 1.17e^{-4} C_K \times H_K$$

As $\sim 0.0117\%$ of all K is the radioactive ^{40}K and H signifies heat production per unit mass (W kg^{-1}) given in Table 1 (based on Jaupart & Mareschal, 2014). Assuming a crustal density of $2,600 \text{ kg m}^{-3}$ (Taylor & Wiecezorek, 2014), this translates to 139 nW m^{-3} at a Th concentration of 1 ppm in the lunar material; with simple linear scaling for other Th (+ U + K) concentrations and/or densities. Therefore, 1 km of typical highlands Th values ($\sim 0.5 \text{ ppm}$), $2,550 \text{ kg m}^{-3}$ material would produce about 0.068 m W m^{-2} surface heat flux, or about 2.3 m W m^{-2} for Wiecezorek et al.’s (2013) 34 km average crustal thickness—which is a reasonable first-order estimate for the crustal production of the average lunar highlands.

Table 1
Main Heat-Producing Isotope Values Used in This Study (Jaupart & Mareschal, 2014)

Isotope	Natural abundance (%)	Heat production per mass (W kg^{-1})	Half-life (year)
^{238}U	99.27	9.17×10^{-5}	4.46×10^9
^{235}U	0.72	5.75×10^{-4}	7.04×10^8
^{232}Th	100	2.56×10^{-5}	1.40×10^{10}
^{40}K	0.0117	2.97×10^{-5}	1.26×10^9

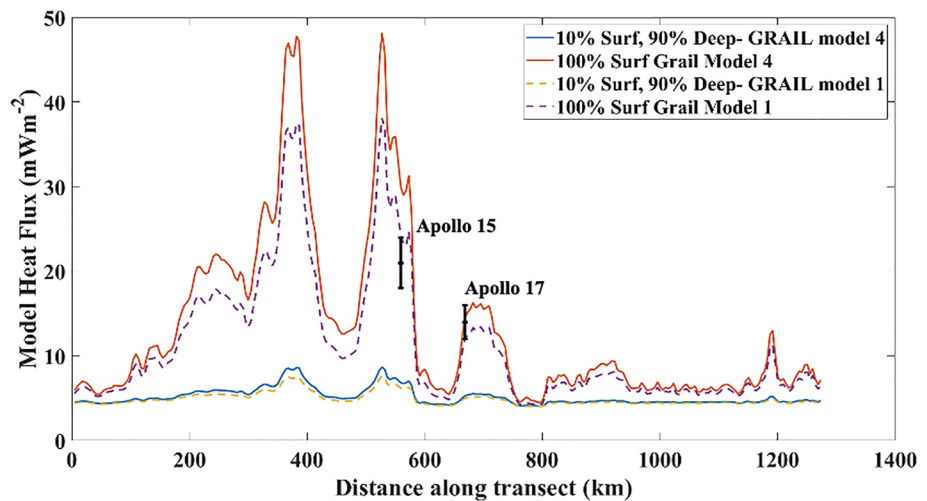


Figure 7. Cross section line connecting Apollo sites for Wieczorek et al. (2013) Model 1 versus Model 4 crust. The solid lines represent the thick crust endmember, Model 4, while the dashed lines represent the thin endmember, Model 1. The upper curves assume the entirety of the crust matches GRS values. In contrast, the lower curves assume only 10% contribution from GRS-like “Surf” regolith composition and 90% “Deep” feldspathic crust with 0.05 ppm Th.

Using this simple framework, we can now produce out high heat flux endmember model for surface heat flux assuming a GRS-derived composition throughout the lunar crust. Figure 6 shows such a model, taking the LP-GRS (with the Warren, 2005 recalibration) surface C_{Th} values (with $C_{Th}/C_U = 3.7$ and $C_K/C_U = 2,000$) as representative of the entire crustal column. Here, the crustal thickness is set by Wieczorek et al.’s (2013) model #4 and crustal density is assumed as $2,550 \text{ kg m}^{-3}$. For now, the model applies a uniform mantle heat flux of 5 m Wm^{-2} (Langseth et al., 1976) at the base and neglects lateral heat flux (addressed in Siegler & Smrekar, 2014).

Here, we can see that this model results (Figure 6) in an extensive range of heat fluxes depending on location with maximum heat fluxes of 95 m Wm^{-2} and minimums (in thin and Th-poor crust) nearing the mantle input of 5 m Wm^{-2} . In this case, the global mean is $\sim 10.5 \text{ m Wm}^{-2}$ and the highlands mean (specified by $C_{Th} < 2 \text{ ppm}$) is $\sim 7.5 \text{ m Wm}^{-2}$. Additionally, this may underpredict heat fluxes at areas with high Th concentrations below out $\frac{1}{4}$ degree ($\sim 7.6 \text{ km}$) model resolution and the $\sim 60 \text{ km}$ (Lawrence et al., 2003) LP-GRS resolution. The highest heat fluxes correspond to a fairly non-distinct area near T. Mayer-A crater near the center of the Procellarum basin, also found to have a low CF in Diviner data indicating relatively silicic composition (Greenhagen et al., 2010), a common feature of many Th “hotspots.” This particular spot shows high in the model because it has a high Th and crustal thickness. Again, it should be noted that there may be other regions in which surface Th (and silicic composition) are hidden from GRS remote sensing techniques by even thin ($\sim 1 \text{ m}$) mare flows and/or ejecta blankets. These thin coverings will result in a cookie-cutter pattern of our heat flow predictions, especially within the lunar mare. The Imbrium basin has relatively low heat flux due to its thin crust and low surface Th concentrations (potentially due to Th-poor basalt fill).

Figure 7 illustrates the straight-line transect (in flat, map-projected space, i.e., not a great circle) of model results through the two Apollo heat flow experiment sites as shown in Figure 6 (as in Siegler & Smrekar, 2014). Zero is simply the intersection with -180° longitude and Apollo 15 and 17 at 560 and 669 km, respectively (noted by the black error bars in Figure 7). The large dip in heat flux at $\sim 450 \text{ km}$ is roughly the center of the Imbrium basin, with two smaller dips being transects through Maria Serenitatis and Crisium. The solid red line represents the surface heat flux predicted from the 100% surface GRS, thickest crustal model (#4), as shown in Figure 7. To illustrate variability, we also plot the same transect through Wieczorek et al. (2013) thinnest model (#1, dashed purple line).

Figure 8 shows the ratio of predicted heat flux between these two endmember crustal thickness models, showing an up to ~ 1.4 ratio in Th-rich areas (note that the difference is negligible in areas of thin crust). Both of these models illustrate that assuming GRS-level concentrations through the entire crust is likely to overpredict the surface heat flow, with the thin model (#1) falling just above values observed at Apollo 15 below values observed

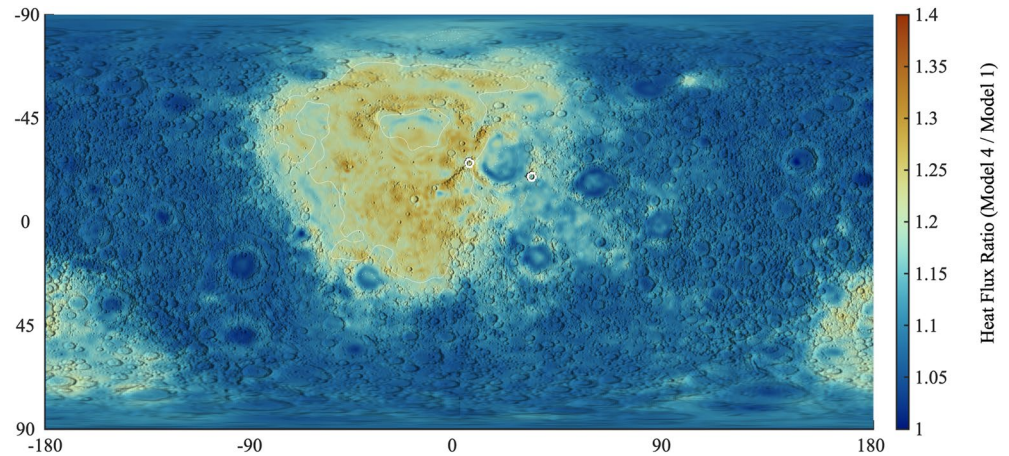


Figure 8. Ratio in full crustal flux heat flux between Wieczorek et al. (2013) model 1 and 4.

at Apollo 17. These concentrations suggest it is impossible to match Apollo 17 crustal heat flux without higher radiogenic concentrations below the visible crust (either from a KREEP layer or higher mantle heat flux). We consequently use model #4 thickness values for the remainder of the paper, but Figure 8 should serve as a conversion factor to the thinner model #1 if desired. Areas in the radiogenic-poor highlands (i.e., between roughly 1,000–1,100 km) show an average of $\sim 6 \text{ m Wm}^{-2}$ in all models, or which 5 m Wm^{-2} is coming from our assumed mantle heat flux. This value highlights how a highlands measurement far from the PKT would strongly constrain mantle heat flux, as will be the planned 2023 Crisium basin mission, which will fly the LISTER heat flow probe (Nagihara et al., 2021; Ngo et al., 2019).

3.1. Layered/Fractional Models

For the next level of model complexity, we create simple models of a surface layer (based on GRS data) and lower crustal FAN layer using the 0.05 ppm Th concentration (Laneuville et al., 2018). We present a series of layered models, in which the surface material represents some globally uniform depth of material, and fractional models, in which some portion of the local crustal column (which varies in thickness) is represented by surface material. We will refer to these two models as the “layered” and “fractional” models for convenience. We continue to assume $C_{\text{Th}}/C_{\text{U}} = 3.7$ and $C_{\text{K}}/C_{\text{U}} = 2,000$ for simplicity. Note that Taylor and Wieczorek (2014) found $C_{\text{K}}/C_{\text{U}} = 1,700$ for this lower crustal material, but the low concentrations of K make this difference negligible. This two-layer model may be rather appropriate for a model where surface radiogenic results from impact mixing of surface pyroxene-rich material with deeper plagioclase-rich material (Laneuville et al., 2018; Taylor & Wieczorek, 2014; Yamamoto et al., 2012). As our heat flux models are one-dimensional, we can be somewhat agnostic about how heat producing elements are actually distributed through the crust—the net column heat production will be the same.

In Figure 7, we see a lower end-member model, assuming the GRS values represent only the upper 10% of the crust that falls well short of the Apollo values (for both crustal thickness models). This model essentially means the surface Th values give little insight into crustal heat production. This also highlights that due to the very thin crust, the 2023 Crisium basin LISTER measurement (Nagihara et al., 2021; Ngo et al., 2019) will not provide much leverage as to the distribution of heat-producing elements in the crust on its own, leaving such questions to be addressed by a global Lunar Geophysical Network (LGN), which should include at least one representative feldspathic highlands measurement (e.g., Neal et al., 2020).

Figure 9a shows transect values for the complete range of crustal radiogenic mixtures. Here, we can see that models where surface GRS-based Th represents 40%–70% of the crust can fit within the bounds of the Apollo 15 heat flux measurements (assuming a minimum 5 m Wm^{-2} mantle heat flux). As both Apollo sites have an approximately 40 km crustal thickness in the “model 4” (of Wieczorek et al., 2013), 40%–70% would be equivalent to approximately 16–28 km of the crust having the same level of radiogenic material as seen in the Apollo HFE locations. For these crustal models to be appropriate for the Moon, deeper radiogenic materials are required

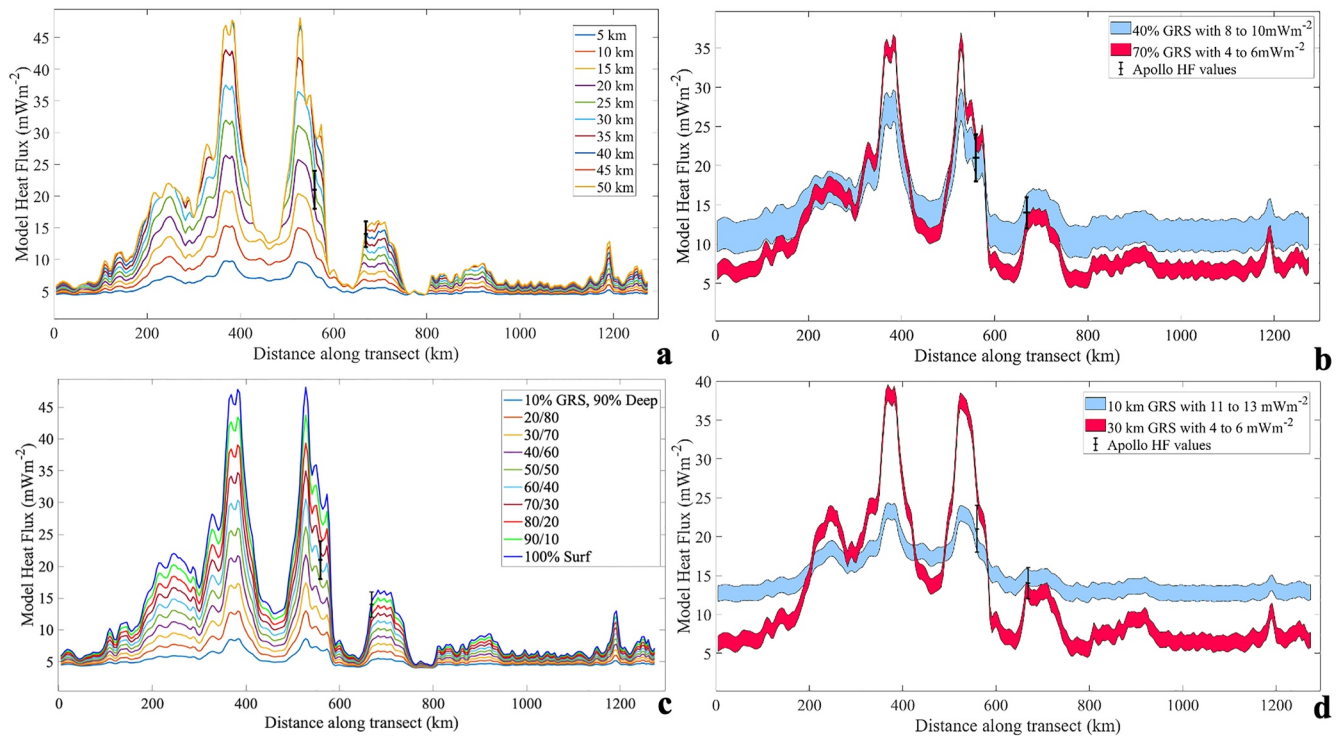


Figure 9. (a, b) Transects of all crustal fraction mixtures show the Apollo 15 and 17 measurements are fit best by a family of ~40%–70% GRS-derived surface heat flux models. (c, d) Transects of all “layered” models show they are fit best by a family of ~10–30 km GRS-derived surface layers with a range of mantle heat flux values.

beneath the Apollo 15 site and at both the Apollo 15 and 17 sites (as was seen in Sieglar & Smrekar, 2014). This observation could be due to a sub-crustal KREEP lens below both sites (e.g., Wiczorek & Phillips, 2000; Laneuville et al., 2018), but more simply can be modeled as an increase in mantle heat flux in our model. We will treat a subcrustal enhancement as a uniform global layer for simplicity.

Figure 9b illustrates the “endmember” range of models that fit the Apollo error bounds with models with 40% GRS-derived heat production requiring larger mantle heat fluxes (8–12 m Wm^{-2}) and models with as much as 70% GRS-derived heat production requiring smaller mantle heat fluxes (4–6 m Wm^{-2}). The variation among such models illustrates the need for measurements in the low-Th highlands and areas of thin crust, such as Mare Crisium, as this differentiates the large variable of mantle heat flux and sheds light on the need for any KREEP-rich layer below Procellarum.

Many models and observations point to a more uniform global mixed layer of higher pyroxene content (and therefore a more Th-rich layer) (Donaldson Hanna et al., 2014; Hawke et al., 2003; Ohtake et al., 2009; Yamamoto et al., 2012) or even a very thin veneer of Th-enriched material (e.g., Taylor & Wiczorek, 2014). This model has some limitations in that the mixed layer can quickly exceed the total crustal thickness in some locations when attempting to apply a global model. Setting such areas of thin crust to be entirely enriched at all depths results in models plotted in Figure 9c, with models of ~15–30 km of GRS-like enriched thickness fitting Apollo 15 values with the nominal 5 m Wm^{-2} mantle heat flux model. Figure 9d shows reasonable bounding models to fit the Apollo error bounds can result in enriched crust depths from 10 to 30 km. Note that these thinner models require a large amount (11–13 m Wm^{-2}) of sub-crustal heat flux, either pointing to a highly enriched mantle or KREEP-rich layer below the PKT. Also, of minor note, assuming surface GRS values, we could not achieve reasonable heat fluxes at both Apollo sites with the ~0–5 km enriched later presented in Taylor and Wiczorek (2014).

4. Birch-Style Interpretation of Existing Heat Flow Data

Another standard way to put limited geothermal measurements into context is to derive a best fit model comparing surface heat flux to surface radiogenic content (e.g., Stein, 1995; Jaupart et al., 2007). This will allow us to compare the Apollo data to models in a more global context. As was first noted by Birch et al. (1968), in regions of Earth's continental crust with relatively simple geology, there sometimes exists a simple linear relationship between radioactive heat source abundance and heat flow:

$$q_0 = q_r + DA_0 \quad (1)$$

where q_0 is the surface heat flow; A_0 is the near-surface radioactive (Th + U + K) heating rate per unit volume; For surface heat production in units of Wm^{-3} D is a slope constant with dimensions of length; q_r is the “reduced” heat flow (units Wm^{-2}) defined by the intercept of the trend at $A_0 = 0$. In the case of the fractional mixing models (Figure 9a and 9b), D is proportionate to the enriched surface mixing ratio.

We use surface Th as measured by LP GRS (for our assumed U/Th/K ratios 1 ppm Th $\approx 1.36 \times 10^{-4} \text{ Wm}^{-3}$). In the case of the mixed-layer models presented in the last section, D , here would be the thickness of the upper surface-Th composition layer, while in the fractional, this depth would vary with crustal thickness. In both cases, q_r represents the deeper low Th anorthositic crust plus the mantle. However, with only 0.05 ppm Th this anorthositic layer produces only about $6.8 \times 10^{-3} \text{ m Wm}^{-2} \text{ km}^{-1}$ (or about 0.27 m Wm^{-2} for the $\sim 40 \text{ km}$ Apollo 15 crust, or about 0.5 m Wm^{-2} for the thickest $\sim 80 \text{ km}$ thick crust in GRAIL model #4), so q_r can be mainly thought of as mantle heat.

On Earth, there are as many as 19 terrestrial “heat flow provinces” that have been observed to reasonably be approximated by the linear relationship (1) as established in the 1980s (e.g., Taylor & McLennan, 1985). Today, authors such as Furlong and Chapman (2013) and Jaupart and Mareschal (2014) caution Birch's heat flow province concept is valid only in selected locales, as Earth's highly processed continental crust as a whole is not as geologically simple. However, we expect the small, long-inactive Moon's crust to be the product of a comparatively simple evolution (cf. the argument of Hahn et al., 2011, regarding the heat-flow geology of Mars). Moreover, interpretational complexity would be hard to justify, given the limitations of the current lunar heat flow data set.

We can use the model results discussed in the previous section to better place an additional constraint on our best fit models and estimate the lunar reduced heat flux. Here, we can represent the Birch-style quantities as surface Th (measured by LP-GRS or our Apollo 15 and 17 lunar sample fits) versus surface modeled (or Apollo HFE measured) heat flux. This plot is seen in Figure 10a, with scatter plots representing model results assuming 10%, 50%, and 100% LP-GRS derived column Th abundance. A linear fit through the accepted Apollo Heat Flow values (14 ± 2 and $21 \pm 3 \text{ m Wm}^{-2}$) provides a slope (DA_0) of 2.92 and intercept (q_r) of 4.96 m Wm^{-2} , noting, however, that intercepts between ~ 11.45 and 0 m Wm^{-2} and slopes of 1.41–4.34 fit within the errors provided by the Apollo values. We find a good fit for this slope using a model with 60% GRS-Th underlain or mixed with 40% column abundance low-Th anorthosite (0.05 ppm Th) and a 5 m Wm^{-2} mantle heat flux, providing a reasonable first-order global heat flux estimate.

Figures 10c and 10d show results addressing the concept of a surface impact-mixed layer enhanced in higher-Th pyroxene. Figure 10c shows layers between 5 and 50 km thick with 5 m Wm^{-2} mantle heat flux, compared to a linear fit through the two Apollo Heat Flow values. If locations had total crustal thickness (Wieczorek model #4 here) less than the enriched layer thickness, the entire crust was assumed enriched (dots falling below the linear trend are areas of thinner crust than the enriched zone—otherwise, these plots would be straight lines). As seen in Figure 9c, thicknesses in the 10–30 km range could provide reasonable fits within error if mantle flux values were allowed to vary. Figure 10d shows the best fit value to the Apollo Heat Flow measurements to be an enriched thickness of 21.5 km, again with a slightly increased 5 m Wm^{-2} mantle flux, providing a similar baseline model to the fractional mixtures. 21.5 km would be about 54% GRS at the $\sim 40 \text{ km}$ thick crust Apollo sites, so the fits are roughly equivalent at these locations. Together, both models point to ~ 20 – 25 km or 55%–60% GRS-level enrichment of the upper crust.

While not explicitly included here due to uncertainties in instrument recalibration that is still in progress, Paige et al. (2016, LPSC) reported on a third potential heat flux constraint from minimum temperatures recorded by the Diviner Lunar Radiometer. Within a small crater at 87.0°S , 15.3°E , this infrared radiometer (Paige et al., 2016)

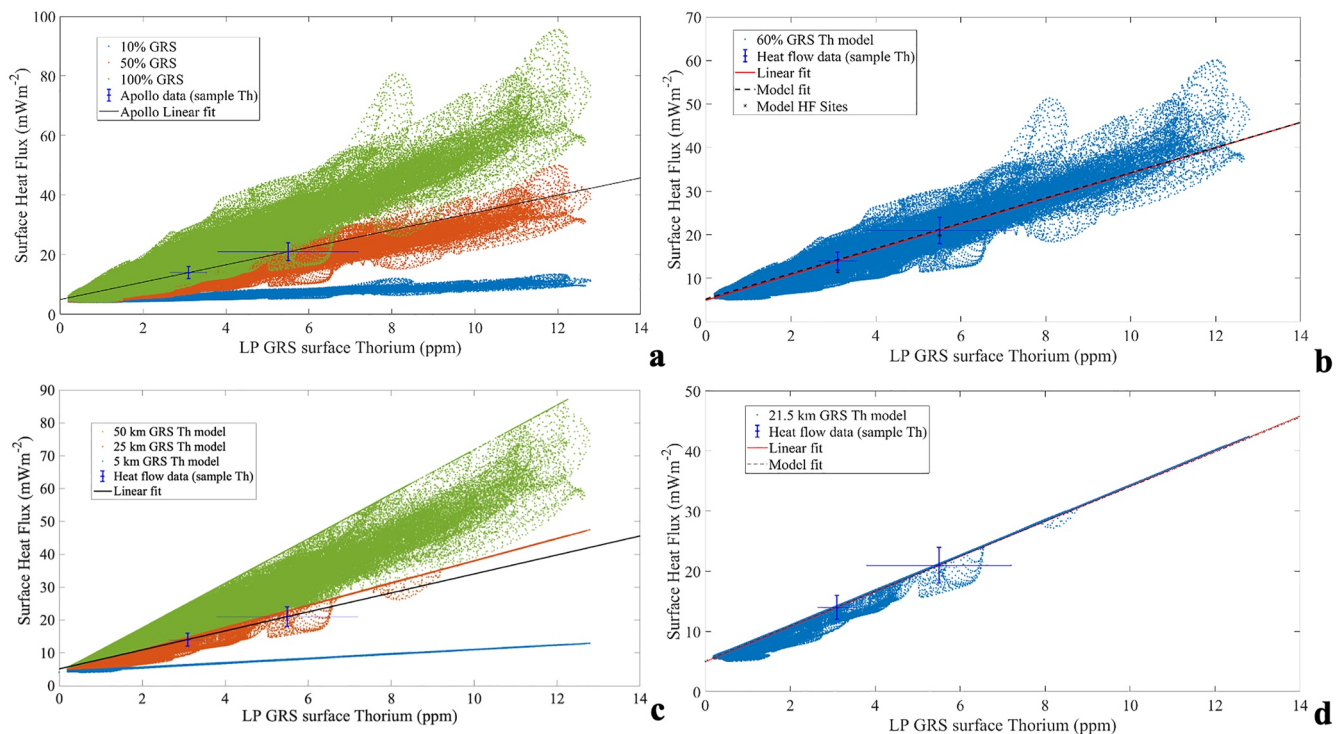


Figure 10. (a) The range of models presented in Figure 9 given a fractional mixture of Lunar Prospector Gamma-Ray Spectrometer (LP-GRS) derived (Lawrence et al., 2003 with Warren, 2005 recalibration) radiogenic content underlain by low Th anorthosite (0.05 ppm Th) below. As in the preceding figures, this plot assumes 5 m Wm^{-2} mantle heat flux. (b) We illustrate a model with 60% LP-GRS mixing and a 5 m Wm^{-2} mantle heat flux, providing a reasonable first-order fit. (c) models for a range of uniform slabs of equal concentration to the surface GRS derived Th underlain by 0.05 ppm Th and 5 m Wm^{-2} mantle heat flux (d) the best-fit model with a 21.5 km thick surface-enriched layer and a 5 m Wm^{-2} mantle heat flux. Note that the models in (c) and (d) are only not straight lines due to the finite thickness of the lunar crust (here following Wieczorek et al. (2013) model #4).

measured surface temperatures were found to dip to a seasonal minimum of $\sim 18\text{K}$, equivalent to $\sim 6 \text{ m Wm}^{-2}$. Coincidentally, this area also has a crustal thickness near the Apollo site's value (39 km in Wieczorek's model #4), but has very low Th concentrations (0.68 ppm). In the fractional fit model, this area results in an expected $\sim 7.1 \text{ m Wm}^{-2}$ and the layered model $\sim 6.1 \text{ m Wm}^{-2}$. While not used for these fits, these values fall remarkably close to our linear fits and lend some credence to the Apollo sites as representative of a global trend. One should note that while this does not on its own exclude the need for a KREEP-rich layer existing below the present-day Procellarum crust, it does not require it. The Apollo sites produce a heat flux consistent with their surface-measured Th when placed globally.

5. Baseline Model for Lunar Surface Heat Flux

From these fits, we can create a first-order baseline model for the expected surface heat flux anywhere on the Moon. Differences from this model would imply that the Apollo sites are more anomalous than their surface Th concentrations alone would imply. To begin with our "fractional model," Figure 11a shows the global results of the fit fractional 60% GRS, 40% "anorthosite" (0.05 ppm Th) mixing model with 5 m Wm^{-2} mantle heat flux. This model shows the highest heat fluxes in Procellarum at approximately 60 m Wm^{-2} , with the lowest values at $\sim 4.8 \text{ m Wm}^{-2}$ in the thin Moscoviense Basin. This could be considered a standard baseline model for expected heat flux and subsequently prove useful for comparison with future lunar measurements.

To also include the "layered model" results, we show Figure 11b. This model is less affected by crustal thickness variations than the fractional model. The 21.5 km surface enriched layer model results in lower maximum values of 33 m Wm^{-2} and a minimum of about 4.5 m Wm^{-2} . Differences up to 25 m Wm^{-2} are found in Th "hot spots" within Procellarum, but these are very localized. Constraining heat flux in one or more of these locations would aid in further differentiating these base models. Relatively minor in the low Th highlands, with values less than

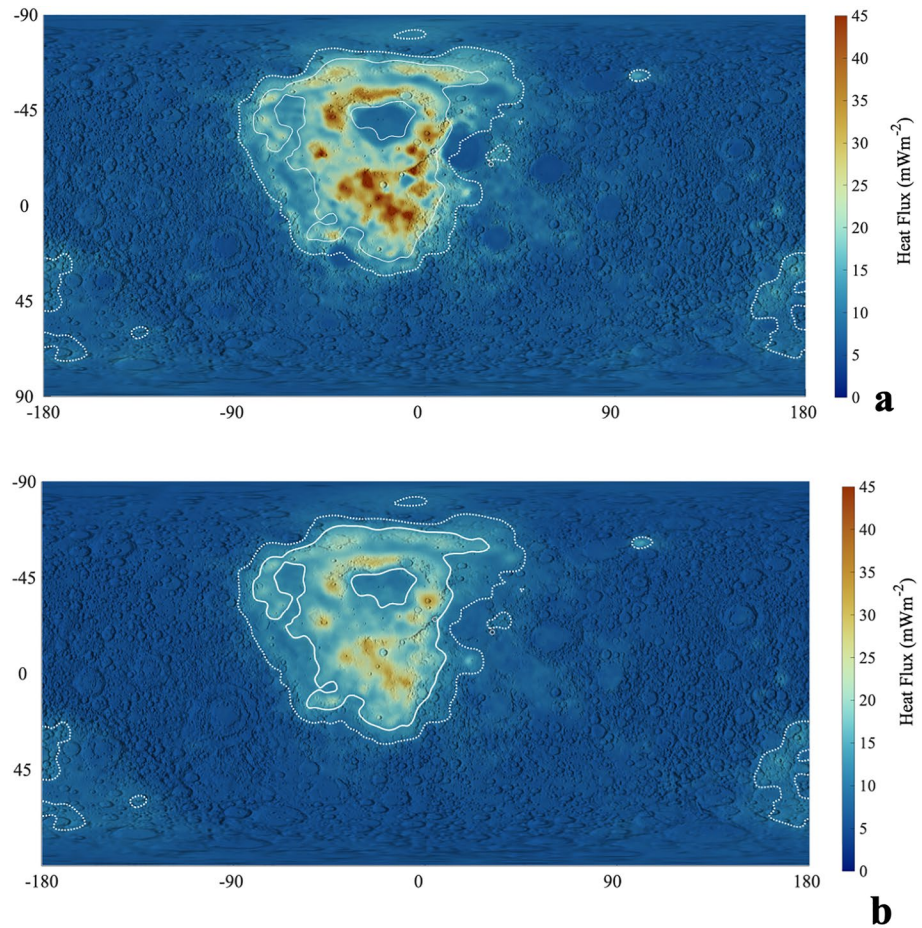


Figure 11. (a) Mapped predicted heat flux model with 60% LP-GRS mixing, now with a 5 mWm^{-2} mantle heat flux, provides a reasonable first-order fit. (b) Predicted heat flux model with a 21.5 km thick surface-enriched layer and a 5 mWm^{-2} mantle heat flux.

1 mWm^{-2} over most of the globe and thus would likely not provide much leverage of differentiating these models from each other.

6. Implications for Bulk Lunar Heat Production and Composition

How reasonable is it to assume that the enriched zone is 60% (or $\sim 21.5 \text{ km}$) and that q_i is uniform at $\sim 5 \text{ mWm}^{-2}$? In terrestrial heat-flow provinces, D (Equation 1) is typically $\sim 10 \text{ km}$, never $> 16 \text{ km}$ (Taylor & McLennan, 1985), and the subsurface Th diminution is commonly assumed to be exponential (Jaupart & Mareschal, 2014). However, as noted by Hahn et al. (2011), on smaller worlds where the potential for intra-crustal secondary differentiation is less, we expect to generally find less pronounced depth-diminution of Th concentration within the crust. So finding $\sim 21.5 \text{ km}$ (which is not coincidentally roughly 60% of the crust at the Apollo sites) to be the enriched zone thickness, or the e-folding thickness in an exponential model, does not seem unreasonable.

As these models provide heat production for the entire lunar crust and mantle, we can use them to provide a sum of all radiogenic heating in the Moon and therefore a total radiogenic content of the Moon. In addition, as future data points are measured, these models can be refined to accommodate that data. As it stands, we can convert our surface-derived heat production values by examining the volume represented by a given pyramidal section of crust in lat/long space (see Appendix A). The heat production of each pyramidal element is then assigned the value required to produce the surface heat flux in that section.

Table 2

Th, U, K, Concentrations or Earth and Moon From Various Estimates/Models

	Th (ppb)	U (ppb)	K (ppm)
Earth Primitive Mantle (McDonough & Sun, 1995)	79.5 ± 11.9	20.3 ± 4.1	240 ± 48
Average Bulk Silicate Earth (BSE)	74 ± 13	20 ± 3.5	400 ± 70
Carbonaceous Chondrite (CI) (McDonough & Sun, 1995)	29	7.4	550
Depleted MORB (Workman & Hart, 2005)	7.9	3.2	25
Average MORB source (Su, 2003; Langmuir & Asimow, 2005)	40	13	160
Continental Crust (Rudnick et al., 2003)	5600	1,300	1.5 × 10 ⁵
Earth Mantle (Turcott and Schubert)	124	31	310
Wieczorek and Phillips (2000) mantle (2.57 m Wm ⁻³ heat flux, Ur ≈ 0.72)	25	6.8	17.6
Our Crust Model, 60% enriched crustal fraction	607	164	328
Our Crust Model, 21.5 km enriched layer	501	135	270
Our Bulk Lunar Model, 60% enriched crustal fraction (assumes mantle all radiogenic, Urey Ratio of 1)	79.02	21.36	42.72
Our Bulk Lunar Model, 21.5 km enriched layer (assumes mantle all radiogenic, Urey Ratio of 1)	73.25	19.80	39.60
Mantle to produce 5 m Wm ⁻³ mantle flux (Urey Ratio of 1)	49.3	13.32	25.64
Mantle, Urey Ratio of 0.72 (e.g., Warren, 2005 mantle)	25.0	6.78	13.5
Mantle, Urey Ratio of 0.65 (average)	19.0	5.14	10.3
Bulk lunar average (our models, assuming C _{Th} /C _U = 3.7, C _K /C _U = 2,000 with assumed 0.65 Urey ratio)	50.5 ± 5.5	13.65 ± 1.49	27.23 ± 2.97

Our fit values result in a total lunar crustal heat production of 1.704×10^{11} W for the fractional case (or 1.633×10^{11} W for the 21.5 km enriched layer case). The common mantle heat flux of 5 mW^{-2} results in 1.807×10^{11} W of mantle heat production. In total, this results in 3.511×10^{11} W for the fractional model (or 3.440×10^{11} W for the layered case), which is reasonably in line with the $\sim 46 \times 10^{12}$ W coming from the Earth (with ~ 9.6 TW from the continents, 34 TW from the oceans, and 3 TW from oceanic “hot spots”) (Jaupart et al., 2007). The use of these values results in about 2.32 times the heat per unit volume, or about $1.59 \times 10^{-8} \text{ Wm}^{-3}$ coming (or about 1.4 times per unit mass, or $4.76 \times 10^{-12} \text{ Wkg}^{-1}$) out of the Earth as compared to the small, faster cooling Moon (which has a roughly 3.7 times higher surface area to volume ratio than the Earth).

However, as with Earth, which is modeled to produce only 20×10^{12} W (20 TW) from radioactive decay (McDonough & Sun, 1995), it is likely that a significant portion of this heat derives from other sources, namely the secular cooling of the body. On Earth, this ~ 26 TW gap between total heat loss and estimated heat production is credited to heat loss from the core (~ 10 TW) and cooling of the hot mantle (~ 16 TW) (Jaupart et al., 2007). Models including core differentiation and contraction credit several TW to these processes, slightly lowering the core and mantle cooling contributions. These deep sources (from the core to the lower crust) of heat will contribute to the derived “reduced heat flux” value. On Earth, older, cooled crustal regions imply a reduced heat flux of $\sim 25 \text{ mW}^{-2}$, while most models suggest Earth’s actual mantle heat production to fall between 11 and 18 mW^{-2} (Jaupart et al., 2007).

Likewise, our $\sim 5 \text{ mW}^{-2}$ lunar reduced value would overestimate the radiogenic content of the lunar mantle, which is also still losing heat, namely from past radiogenic decay. Treating it as an upper limit on mantle radiogenic composition, 5 mW^{-2} would be produced from the mantle with 49.3 ppb Th (again assuming Th/U is 3.7 and K/U is 2,000). Taken as purely radiogenic heat, this would result in a best fit 79.02 ppb Th concentration for the Moon as a whole for the fractional model (73.25 ppb for the layered model), which is remarkably close to estimates of Earth’s primitive mantle (with an average of around 74 ppb Th e.g., McDonough & Sun, 1995; Allègre et al., 2001; Lyubetskaya & Korenaga, 2007; others reviewed in Warren, 2005). These and other radiogenic compositions are summarized in Table 2. However, as some of the mantle heat is likely stored from past radiogenic heat loss, we believe this to be an overestimate. Therefore, from this model, we would expect a Moon with radiogenic composition less than that of the primitive Earth.

We can quantify this potential overestimate with the Urey Ratio, here defined as the ratio of total heat loss to present-day heat production. For example, a purely radiogenic mantle heat production of 5 m W m^{-2} would result in a Urey ratio (U_r , the ratio between the internal heat production and the total surface heat loss) of nearly one (~ 0.97 in both cases). This value is also much higher than expected.

The Urey Ratio is a handy but complex topic of discussion in heat flux literature. There are two families of the Urey ratio: the bulk Urey ratio (which we use here) and the convective Urey ratio (often used to measure the convective strength of the Earth's mantle e.g., Korenaga, 2008). A Urey ratio of one implies that heat production equals heat loss, indicating the average temperature of the mantle would remain constant (Jaupart & Mareschal, 2010). Values above one imply heating of the mantle. Values lower than one suggest a body is cooling, with lower values showing more efficient cooling (likely due to convection). The extreme Urey ratio of 0 corresponds to a situation in which the mantle is fully depleted of all heat producing elements.

Urey ratio estimates for the Earth generally range between 0.21 and 0.49, with favored values around 0.33 (Jaupart & Mareschal, 2010), with the low values in the Earth's case coming from efficient heat loss due to convection and plate tectonics. Mars is modeled to have a higher ratio of around 0.57–0.618 (Plesa et al., 2015), dominated by conductive mantle cooling in the absence of plate tectonics. It is reasonable to expect that the Moon, lacking active tectonics and likely little current mantle convection, should have values also in a similar range to Mars.

The Moon's Urey ratio must be less than one. In models assuming the crust to have uniform thermal conductivity of $2.0 \text{ W m}^{-1} \text{ K}^{-1}$, 120 ppb of bulk-Moon Th, and present-day convection as shallow as 290 km, Schubert et al. (1980) found U_r to be 0.7–0.8. More realistically, cooling of the lunar interior is significantly slowed by the reduced thermal conductivity associated with its porous, brecciated megaregolith. Vacuous porosity causes logarithmic diminution of thermal conductivity (Langseth et al., 1976) by a factor of 10 at 17% porosity. The overall porosity of the lunar crust, estimated from GRAIL data, is 12% (Wieczorek et al., 2013). Warren and Rasmussen (1987) found that a megaregolith of higher porosity but far thinner extent (17%, 8 km; i.e., a comparable total insulating effect) will translate into a reduction of U_r by a factor of ~ 0.93 ; implying 0.65–0.75 as the counterpart to the range found by Schubert et al. (1980). One source has estimated the Moon's U_r is 0.5 (Spohn & Breuer, 2002), but when combined with our estimates, this would imply a mantle with only ~ 3 ppb Th concentration in our models, which may be unfeasibly low.

Based on this literature, we adopt 0.65 for purposes of further interpretation. A Urey ratio of 0.65 would imply a mantle Th concentration of ~ 19 ppb (in both crustal distribution models). Assuming the mantle depth range is ~ 43 km (Taylor & Wieczorek, 2014) to 1407 km (Weber et al., 2011) and its mean density is $3,500 \text{ kg m}^{-3}$ (Konopliv et al., 2013), 19 ppb Th (with standard U/Th/K ratios) equates to a 1.93 mW m^{-2} contribution to surface heat flow q_0 . This portion of surface heat flow would leave roughly 3.07 mW m^{-2} as the portion of q_r deriving from the mantle due to the slow rate of heat loss, implying a bulk lunar Th concentration of 50.84 ppb (for the 60% fractional crust model) or 45.07 ppb (for the 21.5 km layered case).

Independently of this, Wieczorek and Phillips (2000) and Warren (2005) have estimated that the lunar mantle Th concentration averages ~ 25 ppb (this estimate is highly uncertain, but it is a place to start). 25 ppb would imply a $U_r \approx 0.72$. For comparison, Jolliff et al. (2000) argued for 40 ppb. Spohn et al. (2001) estimated 29 ppb. Taylor et al. (2006 GCA) estimated 55 ppb. Thorium contents inferred for pyroclastic glass source regions, ranging from 20 to 400 ppb, led Hagerty et al. (2006) to suggest a much higher bulk-mantle Th content of 150 ppb. With the same mantle thickness, 25 ppb Th (and commensurate U and K) results in 2.53 mW m^{-2} contribution to surface heat flow q_0 . To fit our estimated 5 mW m^{-2} net mantle flux would then require roughly 2.47 mW m^{-2} as the portion of q_r deriving from the mantle due to stored heat. This mantle concentration would imply a bulk lunar Th concentration of 56.42 ppb (for the 60% fractional crust model) or 50.65 ppb (for the 21.5 km layered case).

7. Implications for the Bulk Lunar Composition

In summary, our best estimates based on GRS data and the two Apollo Heat Flow Experiment values provide a bulk lunar composition in the range of 45–56 ppb Th. The associated lunar Urey ratio falls between roughly 0.65 and 0.72. This provides a relatively tight prediction of bulk lunar Th concentration of 50.5 ± 5.5 ppb for our range of crustal models and Urey ratios. To put this in context, Table 2 compares several reported radiogenic concentrations for the Earth and Moon.

50.5 ppb Th falls well below estimates for the composition of the bulk-silicate Earth (BSE; i.e., Earth apart from its metallic core). An average of eight independent estimates (Allègre et al., 2001; Lyubetskaya & Korenaga, 2007; others reviewed in Warren, 2005) indicate BSE with Th ranges of 74 ± 13 ppb. For reasons that remain mysterious, this is significantly higher than the Th concentrations in the silicate portions, Th_{spc} , of most types of chondritic meteorites.

Carbonaceous Chondrites (CI) are generally assigned a relatively low average Th value of ~ 29 ppb (McDonough & Sun, 1995). Combining major-element data from Jarosewich (2006) with trace-element data as compiled by Wasson and Kallemeyn (1988), Th_{spc} among averaged groups of non-CI (LL, L, H, EL, and EH) ranges from 48 (LL) to 55 (H) ppb. The CI show greater diversity, from 46 (CM) to 67 (CV) ppb, but stable-isotopic evidence (Kruijer & Kleine, 2017; Warren, 2011) requires that the Moon and the Earth consist preponderantly of non-carbonaceous materials, with enstatite chondrites ($Th_{spc} = 50$ ppb) showing the closest affinity among the few sampled types (Dauphas et al., 2014).

Thus, our inferred Th_{bm} of 50.5 ± 5.5 ppb is intermediate between an average estimated BSE composition and a chondritic-silicates composition, consistent with both of these materials. Assuming a giant impact origin of Earth, this implies either the proto-Earth was highly differentiated with most material to form the Moon originating from the early proto-Earth mantle or that the impacting body was much more consistent with a chondritic composition. Iron also shows a similar depletion in the Moon (roughly a factor of three depletion in lunar iron, namely in its small core), which has been historically credited to pre-impact differentiation of both the proto-Earth and the Mars-sized impactor. More recent work attributes at least part of this depletion to turbulent mixing within the post-impact disc (e.g., Pahlevan & Stevenson, 2007), which could draw down heavy elements in the Moon-forming vapor cloud. It could be that many of the heavier radiogenic elements (U and Th) were also preferentially drawn into the re-forming Earth.

It is safe to assume our models, based on surface Th values, provide an underestimate of the total crustal heat-producing content of the Moon in certain locations. Mainly, as we discussed earlier in the Apollo 17 section, GRS are likely to underrepresent the actual column Th abundances in areas with recent resurfacing by the low-Th mare. In this respect, the models presented here could be viewed as a minimum heat production. Additionally, many well-grounded theoretical models predict highly radiogenic enhancements in or below the lower crust (Laneuville et al., 2013; Warren & Wasson, 1979; Wiczorek & Phillips, 2000) and are beyond the scope of this discussion. As the lunar magma ocean differentiates, olivine and pyroxene form Th-poor mafic cumulates. Subsequently, Th-poor plagioclase would float to form the crust with the primitive lunar crust progressively enriched in Th with depth. Finally, the last melt would concentrate in the liquid layer sandwiched between them and create the KREEP-rich lithologies. If it has never interacted with the surface, it would not appear in this model and would only be observable through its geophysical signature and most readily observed via geothermal heat flux measurements.

If such deep crustal or sub-crustal highly radiogenic material is present, the question is then whether it is present globally or concentrated within the Procellarum region. Gravity measurements (Andrews-Hanna et al., 2014; Wiczorek et al., 2013), crustal magnetism (e.g., Laneuville et al., 2018), electrical conductivity sounding (Grimm, 2013), and past models of True Polar Wander (Siegler et al., 2016) are all consistent with a large concentration of heat-producing elements within or below Procellarum. Still, a global deep crustal enhancement remains unconstrained (e.g., Taylor & Wiczorek, 2014). We do not intend to conjecture if such deeper radiogenic enhancements exist, but utilizing the current heat flux data, we can make a reasonable global model without directly evoking them. For example, adding a 5 km KREEP layer at the base of the PKT region crust (as was done in Siegler & Smrekar, 2014) would simply add ~ 10.21 m Wm^{-2} to our surface heat fluxes in that region. A properly distributed heat flux network would be a primary way to observe such deep crustal enhancements.

8. Implications for Heat Flux Measurements and Landing Site Selection

These models provide an initial expectation for the surface heat flux of the Moon. Ideally, one would measure geothermal heat flux at every point on the Moon. However, this is a feat that is far from being accomplished on the Earth, let alone the Moon. A comprehensive, globally distributed network should be derived from representative regions with varied crustal surface radiogenic compositions and crustal thicknesses. Several mission studies,

such as the LGN or International Lunar Network (ILN), (e.g., Cohen et al., 2008; Neal et al., 2010, 2020) have proposed such globally distributed measurements.

As a first step toward this goal, the LISTER heat flow probe (Nagihara et al., 2021) on the planned 2023 Crisium Blue Ghost lander (which will coincidentally fall at ~ 770 km along the transect in Figures 7 and 9). This probe will take temperature measurements in the upper 3 m of the lunar regolith to provide a geothermal gradient (Nagihara et al., 2021). Crisium is one of the thinnest areas of crust on the Moon (~ 5 – 7 km) and has low surface Th. Therefore, Crisium should provide a strong constraint on mantle heat production, but it may be too thin to constrain the effects of crustal radiogenic content. A duplicate of this instrument was the recently selected heat flow probe to the far side Schrodinger basin and will examine a region of slightly thicker crust than Crisium (~ 15 km in the central basin, ~ 30 km in the outer ring) with similar surface GRS Th values, providing leverage on the 60% and/or 21.5 km model fits in areas far from Procellarum.

These two compelling measurements will significantly advance our ability to constrain models of lunar composition. Additionally, these missions will provide a strong tie point on heat flux coming from the lunar mantle and notably constrain the reduced heat flux intercept in the Birch-style interpretation. The Apollo Heat Flow Experiment locations provide intermediate-Th values, but their anomalous locality near the edge of the compositionally anomalous Procellarum basin leaves some ambiguity (e.g., Neal et al., 2020, PMCS). This leaves a clear missing phase space of high surface Th areas (>8 ppm Th), most of which lie within highlands terrain found inside of the Procellarum basin. However, if the “Moon as a single province” concept holds, these locations should all fall roughly along a line in Birch-style plots like Figure 10 (when corrected to the ~ 40 km crustal thickness of the two Apollo HFE sites).

However, this begs a fundamental question: is it appropriate to treat the Moon as a single heat flow province? As discussed in the previous section, the major unknown is whether the lunar surface Th genuinely represents the bulk crust. This potentially sets the Procellarum region apart as it may have higher radiogenic contributions from a sub-crustal (e.g., Wieczorek & Phillips, 2000; Siegler & Smrekar, 2014) or lower-crustal (Grimm, 2013; Laneville et al., 2013, 2018; Siegler et al., 2016) KREEP-rich layer. Also, the entirety of the crust may have unseen LKFM basalt (low-K Fra Mauro) layer of varying thickness (Taylor & Wieczorek, 2014). Nevertheless, as was done in that study, we can make some headway in breaking the Moon up into what may be separate lunar heat flow provinces.

These heat flow provinces should be separated such that at least one measurement in each province class would provide a representation of the Moon as a whole. In other words, if a specific province class were measured, it would be a higher mission priority to measure a different type of terrain rather than repeat a similar measurement. For instance, the planned 2022 Firefly mission to Crisium will land in an area with distinctively thin crust and low Th. This heat flux measurement is likely to be representative of most similar highland measurements with a thin crust. Therefore, we group all such areas into a single heat flux province (Class 1).

Figure 12 and Table 3 illustrate an attempt to separate the lunar surface into seven distinct classes. Please note that these classes are based on a $1/4^\circ$ interpolation of ~ 50 km resolution Th data (Lawrence et al., 2003) and may not precisely align with geological boundaries.

The first three classes represent the highlands of the Moon, separated by crustal thickness with somewhat arbitrary cutoffs of 20 and 50 km (using Wieczorek et al., 2013 model #4) separating them. Class 1, as discussed above, are areas with very thin crust and low surface Th. These are likely windows into the composition of the mantle from a heat flow perspective and should be high priority targets for constraining bulk lunar composition. Class 1 is represented by the upcoming Crisium basin LISTER heat flux measurement, slated for 2023. If the 2025 Schrodinger Basin version of this instrument lands within the central ring, it would also represent Class 1. Still, it could be used to examine if there is global variation in mantle composition and strengthen the Crisium measurement.

The cutoffs for the remaining highland classes, 2 and 3, roughly follow the “outer, O” and “inner, A” FHT separation suggested in Jolliff et al. (2000), respectively. Class 2 (approximately equivalent to FHT, O) was separated by Jolliff et al. (2000) as it appeared to have higher contamination (both in FeO and in Th) from basin ejecta as compared to the more purely anorthositic Class 3 (approximately equivalent to FHT, A). As this separation is seen both in surface contamination and crustal thickness, we can imagine that these terrains could show slight

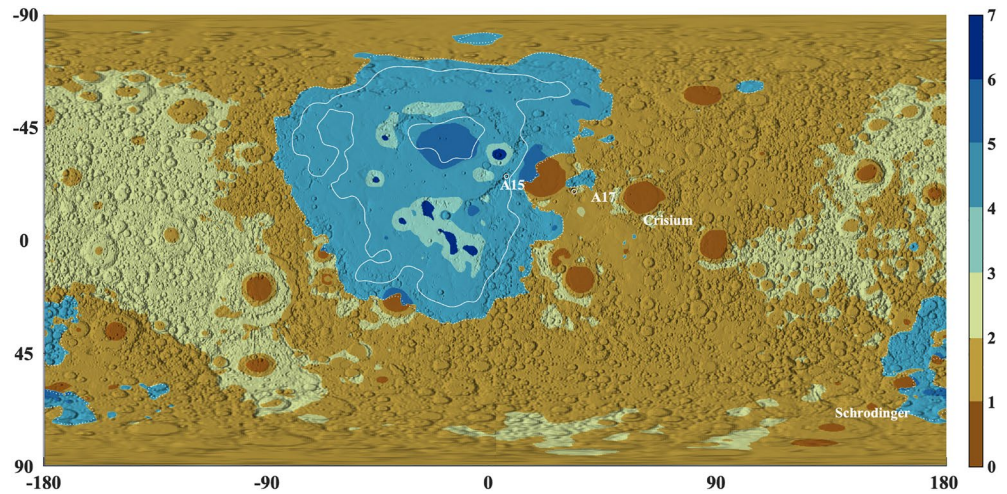


Figure 12. Heat Flow Provinces of the Moon. Based on crustal thickness and surface Th values, we break the Moon into seven potential “heat flow classes”, based on crustal thickness and surface Th concentrations. Classes are detailed in Table 3 with (Class 1) Dark Blue, (2) Blue, (3) Light Blue, (4) Aqua, (5) Tan, (6) Light Orange, and (7) Dark Orange. White dashed lines mark 2ppm Th, solid lines 4ppm Th.

Table 3

Suggested Heat Flow Province Classes as Mapped in Figure 12

Class	Needed Measurement	Constraint Supplied	Representative Mission or province	Surface Th %	Model Heat Flux %	Areal % of Moon	Volume % of Crust	Average Crustal Thickness	Average Heat Production
Class 1	Thin (<20km), low Th Highlands Crust	Mantle composition constraint	LISTER, Crisium ~2023 LISTER, Schrödinger ~2025 (if Inner ring)	1.74%	1.48%	2.29%	0.65%	12.6 km	1.465e-7 W/m ³
Class 2	Medium (20-50km), low Th Highlands Crust	Highlands and Lower Crustal MG suite	LISTER, Schodinger ~2025 (if Outer ring) Apollo 17 (border)	26.78%	40.85%	52.4%	48.30%	39.9 km	9.767e-7 W/m ³
Class 3	Thick (>50km), low Th Crust	Highlands and Lower Crustal composition	Far-side Highlands	6.42%	18.49%	25.9%	33.91%	57.4 km	4.884e-8 W/m ³
Class 4	PKT, high Th		Procellarum region highlands	11.44%	6.31%	1.79%	1.55%	38.1 km	7.475-7 W/m ³
Class 5	PKT (or SPA), low Th	Heat Production below Mare	Apollo 15 Apollo 17 (border)	49.12%	30.64%	16.3%	13.60%	34.1 km	5.467-7 W/m ³
Class 6	PKT (or SPA), Thin Crust	Presence of sub-crustal KREEP layer	Imbrium basin	2.47%	1.08%	1.10%	0.42%	16.5 km	4.328e-7 W/m ³
Class 7	Anomalous hot spots/volcanic	Crustal enriched “plutons”	Potential Gruithuisen Domes ~2025; Aristarchus	2.02%	1.14%	0.25%	0.23%	40.3 km	1.567e-6 W/m ³

differences in heat flux. This will especially be the case if there is a hidden lower crustal radiogenic component (e.g., “LKFM basalt,” low-K Fra Mauro, Taylor & Wieczorek, 2014) that varies with total crustal thickness. Such a deep LKFM basalt layer is not represented in our models, causing model predictions for Class 2 and 3 to be similar beyond a slight Th increase nearing the PKT. If the Schrödinger Basin heat flux measurement is within the outer ring, it will represent Class 2.

Classes 4–6 fall within the PKT or South Pole–Aitken (SPA) basin. One could certainly argue that PKT and SPA terrain be separated, as was done in Taylor and Wieczorek (2014) or Jolliff et al. (2000). In the PKT, Class 4 generally represents the “highlands islands,” or areas of high-Th PKT that are generally higher elevation and were not covered by the lower-Th mare basalts. These “islands” likely provide the clearest look into the composition of the PKT crust from the surface. Class 5 PKT regions are generally locations where relatively thin basalts (<500 m; Du et al., 2019) likely cover higher Th crustal materials. The Apollo 15 and arguably the Apollo 17 site (borders Class 5 and 2) would fall in this zone. Class 6 areas have a thin crust and may provide windows into the presence of lower crustal enrichment below the PKT. For instance, a measurement within the Imbrium basin would provide substantial leverage as to the presence of a sub-crustal KREEP layer (as in Wieczorek & Phillips, 2000) or LKFM layer (as in Taylor & Wieczorek, 2014) in this region and provide a strong constraint on any compositional differences in the PKT region mantle.

Class 4 is absent in the SPA due to lower Th values there. In the SPA basin, where there is little mare, Class 5 areas have surface Th values that should represent the crust below. Class 6 will again provide a strong constraint on the presence of an LKFM layer below SPA of any anomalies in mantle composition in this region.

Class 7 removes Th hot spots, which generally correspond with areas of suggested silicic volcanism (e.g., Glotch et al., 2010) and are likely linked to localized crustal remelting and concentration of Th. All mapped here fall within the PKT. Due to the resolution to which we have gridded here ($\sim 1/4^\circ$), we should note that the farside Compton-Belkovich Th hot spot does not appear on this map, but would also represent Class 7, though likely with a different origin than the PKT locations. Though they are high heat flux, these hot spots do not dominate the heat loss of the Moon, representing $\sim 2\%$ of the surface Th and 1.15% of our total model calculated surface heat loss and represent only $\sim 0.23\%$ of the total volume of the crust. While these are fascinating spots geologically, they are anomalies that are not representative of global heat production.

Table 3 shows an accounting of the fraction of the total surface Th, model heat flux (from the layered model here), fractional area, and fractional crustal volume represented by each province. We see that most of the Moon ($\sim 95.8\%$ of the crustal volume and $\sim 90.0\%$ of the modeled heat flux) falls in Classes 2, 3, and 5. This implies that such regions should be the priorities in constraining the total flux from the lunar crust. These classes will also greatly constrain the existence of lower crustal heat production increases that are not directly represented on the surface (e.g., LKFM, Taylor & Wieczorek, 2014; Sub-PKT KREEP, Wieczorek & Phillips, 2000). A SPA basin Class 5 measurement would also look into deeper LKFM materials suggested in this region (Taylor & Wieczorek, 2014).

Class 1 then serves as a needed counterpart for constraining the separate constraint of mantle heat flux in the relative absence of thick crust. Class 6 provides a similar crustal window to the PKT-region mantle (and plausibly sub-crustal PKT KREEP layer; Wieczorek & Phillips, 2000). Class 1 has been prioritized with the 2022 Crisium Basin LISTER heat flux measurement, which should significantly enhance our understanding of the bulk lunar mantle.

The remaining classes 5 and seven offer scientifically interesting windows into late-stage volcanism on the Moon, but they may not provide clear windows into the global bulk composition. Nevertheless, it is plausible that some locations in Class 7, modeled to provide over 50 m Wm^{-2} heat flux, could provide means of geothermal power/heating resources for future exploration.

Future lunar heat flow measurements should be aimed to sample the diversity of these regions with the suggested priority:

1. **Class 2:** The highest priority target would be Class 2 (moderate crust highlands) as it represents nearly half of the crust of the Moon by volume and 41% of the Moon by crustal heat production in our model. Measurements in this region would strongly anchor models like the one developed here. Ideally such a measurement would be paired with a Class 1 (thin crust highlands) to provide a constraint on the mantle contribution to the total

- heat flux and a Class 3 measurement to provide a “Birch plot” for the highlands, but alone, this could provide a valuable constraint on crustal composition of the Moon outside the PKT. Depending on the exact landing site, an outer-ring measurement could provide a potential Class 2 constraint.
2. **Class 1:** The next priority would be to separate mantle from crustal heat flux, which is best done with a Class 1 measurement, having minimal crustal contribution. The planned heat flux measurements at the 2023 Crisium basin are an ideal location for this. An inner-ring Schrodinger Basin measurement could search for plausible variations in mantle heat production near SPA.
 3. **Class 5:** This Class represents the next largest fraction of the lunar crust, including about 16% of the crustal volume and 31% of the crustal heat production. Characterizing this broader PKT region will elucidate how representative the dramatic surface increase in Th seen in the PKT is of the crustal column below. This would also aid in highlighting the potential presence of a large KREEP layer below the PKT (e.g., Wieczorek & Phillips, 2000). The two existing Apollo measurements are roughly sample Class 5, but maintain sufficient geologic ambiguity to motivate future measurement targets for this heat flux class. The far-side SPA Class 5 may be very different than that in the PKT and could be considered a separate target.
 4. **Class 6:** The Imbrium Basin dominates this class and would arguably follow in priority as a direct measure of the present-day existence of a KREEP-rich layer below the Procellarum crust. This heat source has been credited for the presence of the mare (Laneuville et al., 2013, 2018; Wieczorek & Phillips, 2000), magnetic, and electrical properties anomalies (Grimm, 2018; Wieczorek, 2018), and true polar wander (Siegler et al., 2016). However, it is unknown if it truly existed and remains below or within the crust today, or was redistributed throughout the PKT by impact excavation (Hagermann & Tanaka, 2006; Haskin, 1998; Siegler & Smrekar, 2014). A Class 5 measurement does not differentiate crustal from subcrustal KREEP, but the thin Imbrium region would. Our model does not include a sub-crustal KREEP layer, resulting in the Imbrium basin’s “low” ($\sim 8.5 \text{ m Wm}^{-3}$) heat flux. However, the presence of a KREEP underplating under the PKT would make this one of the higher heat flux locals on the Moon (at ~ 18.7 and 28.9 m Wm^{-2} for a 5 or 10 km thick KREEP layer, respectively). An Imbrium basin measurement would provide a strong constraint of any sub-crustal KREEP layer. Such a concentrated KREEP layer could dramatically affect estimates of bulk lunar composition.
 5. **Classes 3 and 4:** Class 3 and 4 regions reveal information about the lower crustal radiogenic composition, potentially increasing the bulk lunar radiogenic composition. In most models of lunar crustal formation going back to Ryder and Wood (1977), the lower crust solidifies last, preserving a more mafic, radiogenic-rich composition. We have not directly included such an increase in lower crustal radiogenic concentration in this model, but rather simply claimed the crustal column Th concentrations are directly proportionate to those seen on the surface. This model is agnostic to that Th being near the surface or in the lower crust. Global heat flux measurements, especially in Class 3 and 4 regions, could reveal if lower crustal radiogenic concentrations vary separately from their expression at the surface. We set them as a lower priority as they would be most applicable as comparative measurements to Class 2 and 5 locations, examining how heat flux varies with total crustal thickness. Class 4 regions may also reveal the continued presence of a Procellarum region KREEP-rich layer, but with a more complex interpretation than Class 6 would provide.
 6. **Class 7:** The remaining Class 7 Th “hotspots” are arguably the most interesting sites to measure heat flux from a geologic perspective as they are generally coincident with the latest stage volcanism on the Moon. Here, we list them as a lower priority as we aim to understand the bulk lunar composition. However, we do not intend to diminish measuring their heat flux as important to lunar science. These locations likely represent highly reprocessed areas of crust, which concentrated both silicate and radiogenic-rich materials. This crustal remelting is an important marker of the end-stage processes of lunar thermal evolution. Despite their highly radiogenic concentration, their small extent leaves them small components in the total lunar heat production.

Figure 13 illustrates the temperature profiles resulting from the average crustal column (in terms of heat production and crustal thickness, as noted in Table 2). Here, each crustal column is split into two layers, with the upper 60% of the crustal thickness in Table 2 being represented being given heat production value also given in Table 2. The lower 40% is given an anorthite representative $5.00 \times 10^{-8} \text{ Wm}^{-3}$ heat production. Mantle material fills the remaining depth to 150 km with $4.52 \times 10^{-9} \text{ Wm}^{-3}$ heat production and 5 m Wm^{-2} heat flux at its base.

These profiles are generally cooler than published models (e.g., Siegler & Smrekar, 2014) due to our lower derived mantle heat flux and lower crust being composed of low Th anorthosite. These models do not include a sub-crustal KREEP layer as discussed in previous work (Laneuville et al., 2013, 2018; Siegler & Smrekar, 2014;

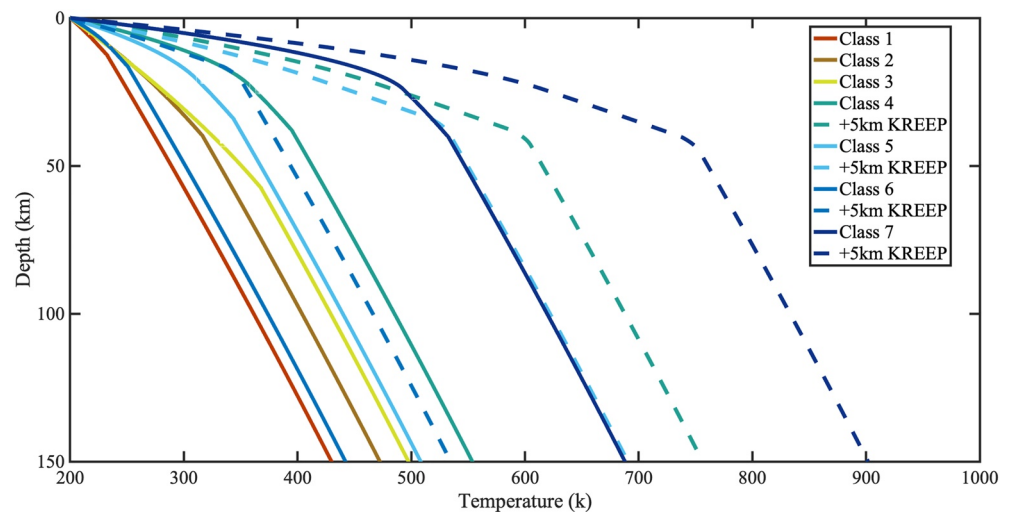


Figure 13. Heat Flow Provinces of the Moon. Based on crustal thickness and 60% surface Th values throughout the crust. We break the Moon into seven potential “heat flow classes” based on crustal thickness and surface Th concentrations. Classes are detailed in Table 3 with (Class 1) Dark Blue, (2) Light Blue, (3) Green, (4) Black instead of yellow for visibility, (5) Orange, (6) Red, and (7) Dark Red. Dashed lines are predicted temperatures in the presence of a 5 km KREEEP layer at the base of the crust.

Wieczorek & Phillips, 2000). If a 5 km KREEEP layer (with $2.042 \times 10^{-6} \text{ Wm}^{-3}$ heat production) were added to the base of the crust for the PKT region (Class 4–7) models, temperature profiles would instead resemble the dashed lines in Figure 13. A global seismic, heat flux, and electromagnetic network spanning the provinces discussed would be a powerful tool in differentiating these temperature profiles. Similarly, if a more radiogenic rich LKFM layer underplates the highlands (Classes 2 and 3), subsurface temperatures would also be enhanced in these regions.

9. Conclusions

The models discussed in this paper provide a benchmark for comparing future surface heat flux measurements to existing data and provide a framework of target regions that can aid in constraining global heat production of the Moon. With current data, the global heat flux of the Moon can be considered as a single heat flux province, in which surface heat flux and surface radiogenic heat production show a direct, linear relationship (following Birch et al., 1968; Langseth et al., 1976; Stein, 1995). However, as more data is taken, the Moon may be divided into several distinct heat flux provinces, with a general categorization suggested in Section 7.

The current, best-fit, linear “Birch model” shows a consistent story with global heat fluxes represented by $\sim 60\%$ surface Th value or equivalently a 21.5 km thick layer with surface Th values. The zero-thorium intercept, or “reduced heat flux,” of these models is approximately 5 m Wm^{-2} , implying the net heat flux from the mantle is at or below this value. With an estimated Urey ratio between 0.65 and 0.725, this equates to a mantle thorium concentration of $\sim 19\text{--}25$ ppb.

This model suggests a bulk thorium concentration of approximately 50.5 ± 5.5 ppb. This value is based on the heat flux that would be obtained from a $C_{\text{Th}}/C_{\text{U}} = 3.7$, $C_{\text{K}}/C_{\text{U}} = 2,000$ or equivalently 13.65 ± 1.49 ppb of uranium and 27.23 ± 2.97 ppm potassium. This value is intermediate between an average estimated BSE composition and a chondritic-silicates composition. It would imply that either the proto-Earth was mostly differentiated with most material to form the Moon originating from the early proto-Earth mantle.

However, the models presented here are only constrained by the two Apollo heat flow measurements (Langseth et al., 1976) and may not apply globally if higher radiogenic concentrations underplate the surface, likely requiring further heat flux measurements to confirm or refute. The existence of a postulated sub-crustal LKFM or PKT-region KREEEP layer would show enhancements over this model in both surface heat flux and subsurface temperatures, suggesting this model serves as a lower limit on lunar heat flux.

The presence or absence of non-surface heat-producing material not represented on the surface would be constrained by new measurements in distinct heat-producing regions. We outline these regions and prioritize their importance for different lunar science goals in differentiating compositional variations in the lunar crust and mantle. Additionally, we provide nominal thermal profiles that may apply to variations in seismic velocities and historic volcanism across the Moon.

Appendix A: Volume of a Section of Crust

The volume of a pyramid (also any cone) is $V = \frac{1}{3}bh$, where b is the area of the base and h the height from the base to the apex. Therefore, the volume of a piece of the crust could be represented by:

$$V_c = \frac{1}{3}b_s R - \frac{1}{3}b_m(R - d)$$

where b_s is the surface area of the piece of the lunar crust and b_m is the bottom area. R is the radius of Moon and d is the thickness of lunar crust. The b_s is calculated from:

$$b_s = \frac{1}{n}L \times \frac{1}{n}L \times \cos\varnothing$$

where \varnothing is the latitude of the piece of lunar crust, n is the resolution, and L is the length per degree with $L = 2\pi R/360$. The bottom area is: $b_m = \left(\frac{R-d}{R}\right)^2 b_s$

Then we have $V_c = \frac{1}{3}b_s R - \frac{1}{3}b_s \left(\frac{R-d}{R}\right)^2 (R - d) = \frac{1}{3}b_s \frac{R^3 - (R-d)^3}{R^2} = \frac{1}{3} \frac{1}{n^2} \left(\frac{2\pi}{360}\right)^2 (R^3 - (R - d)^3) \cos\varnothing$.

Data Availability Statement

Data for Figures 11a, 11b and 12 are archived in Siegler (2022). The primary data used for this modeling are the GRAIL Crustal Thickness Archive (Wieczorek, 2012) and the Lunar Prospector Gamma Ray Spectrometer thorium data set, available at the Lunar Prospector GRS Elemental Abundance Bundle (Prettyman, 2021).

Acknowledgments

This work was funded by NASA grants from the Lunar Reconnaissance Orbiter project Grant NNG09EK06C16 and Solar System Observations Grant NNX17AF12G as well as the Planetary Mission Concept Study NNH18ZDAOQ1N for the Lunar Geophysical Network. We thank our reviewers and the editorial staff for greatly improving the paper.

References

- Allègre, C., Manhès, G., & Lewin, E. (2001). Chemical composition of the Earth and the volatility control on planetary genetics. *Earth and Planetary Science Letters*, 185(1–2), 49–69. [https://doi.org/10.1016/S0012-821X\(00\)00359-9](https://doi.org/10.1016/S0012-821X(00)00359-9)
- Andrews-Hanna, J. C., Asmar, S. W., Head, J. W., III, Kiefer, W. S., Konopliv, A. S., Lemoine, F. G., et al. (2013). Ancient igneous intrusions and early expansion of the Moon revealed by GRAIL gravity gradiometry. *Science*, 339(6120), 675–678. <https://doi.org/10.1126/science.1231753>
- Andrews-Hanna, J. C., Besserer, J., Head, J. W., III, Howett, C. J., Kiefer, W. S., Lucey, P. J., et al. (2014). Structure and evolution of the lunar Procellarum region as revealed by GRAIL gravity data. *Nature*, 514(7520), 68–71. <https://doi.org/10.1038/nature13697>
- Besserer, J., Nimmo, F., Wieczorek, M. A., Weber, R. C., Kiefer, W. S., McGovern, P. J., et al. (2014). GRAIL gravity constraints on the vertical and lateral density structure of the lunar crust. *Geophysical Research Letters*, 41(16), 5771–5777. <https://doi.org/10.1002/2014gl060240>
- Birch, F., Roy, R., & Decker, E. (1968). Heat flow and thermal history in New England and New York. In E.-A. Zen, W. S. White, J. B. Hadley, & J. B. Thompson (Eds.), *Studies of Appalachian geology: Northern and maritime* (pp. 437–451). Interscience.
- Cahill, J. T. S., Lucey, P. G., & Wieczorek, M. A. (2009). Compositional variations of the lunar crust: Results from radiative transfer modeling of central peak spectra. *Journal of Geophysical Research*, 114(E9), E09001. <https://doi.org/10.1029/2008je003282>
- Cohen, B., Bessler, J. A., Harris, D. W., Hill, L., Hammond, M. S., McDougal, J. M., et al. (2008). The International Lunar Network (ILN) and the US Anchor Nodes mission. In *Update to the LEAG/ILWEG/SRR*, 30.
- Dauphas, N., Burkhardt, C., Warren, P., & Fang-Zhen, T. (2014). Geochemical arguments for an Earth-like Moon-forming impactor. *Philosophical Transactions of the Royal Society A: Mathematical, Physical & Engineering Sciences*, 372, 20130244. <https://doi.org/10.1098/rsta.2013.0244>
- Donaldson Hanna, K. L., Cheek, L. C., Pieters, C. M., Mustard, J. F., Greenhagen, B. T., Thomas, I. R., & Bowles, N. E. (2014). Global assessment of pure crystalline plagioclase across the Moon and implications for the evolution of the primary crust. *Journal of Geophysical Research: Planets*, 119(7), 1516–1545. <https://doi.org/10.1002/2013je004476>
- Du, J., Fa, W., Wieczorek, M. A., Xie, M., Cai, Y., & Zhu, M. H. (2019). Thickness of lunar mare basalts: New results based on modeling the degradation of partially buried craters. *Journal of Geophysical Research: Planets*, 124(9), 2430–2459.
- Dygart, N., Lin, J. F., Marshall, E. W., Kono, Y., & Gardner, J. E. (2017). A low viscosity lunar magma ocean forms a stratified anorthitic flotation crust with mafic poor and rich units. *Geophysical Research Letters*, 44(22), 11–282. <https://doi.org/10.1002/2017gl075703>
- Feldman, W. C., Barraclough, B. L., Fuller, K. R., Lawrence, D. J., Maurice, S., Miller, M. C., et al. (1999). The Lunar Prospector gamma-ray and neutron spectrometers. *Nuclear Instruments and Methods in Physics Research Section A: Accelerators, Spectrometers, Detectors and Associated Equipment*, 422(1–3), 562–566. [https://doi.org/10.1016/S0168-9002\(98\)00934-6](https://doi.org/10.1016/S0168-9002(98)00934-6)

- Furlong, K. P., & Chapman, D. S. (2013). Heat flow, heat generation, and the thermal state of the lithosphere. *Annual Review of Earth and Planetary Sciences*, 41(1), 385–410. <https://doi.org/10.1146/annurev.earth.031208.100051>
- Gagnepain-Beyneix, J., Lognonné, P., Chenet, H., Lombardi, D., & Spohn, T. (2006). A seismic model of the lunar mantle and constraints on temperature and mineralogy. *Physics of the Earth and Planetary Interiors*, 159(3–4), 140–166. <https://doi.org/10.1016/j.pepi.2006.05.009>
- Gillis, J. J., Jolliff, B. L., & Korotev, R. L. (2004). Lunar surface geochemistry: Global concentrations of Th, K, and FeO as derived from lunar prospector and Clementine data. *Geochimica et Cosmochimica Acta*, 68(18), 3791–3805. <https://doi.org/10.1016/j.gca.2004.03.024>
- Glotch, T. D., Lucey, P. G., Bandfield, J. L., Greenhagen, B. T., Thomas, I. R., Elphic, R. C., et al. (2010). Highly silicic compositions on the Moon. *Science*, 329(5998), 1510–1513. <https://doi.org/10.1126/science.1192148>
- Gong, S., Wieczorek, M. A., Nimmo, F., Kiefer, W. S., Head, J. W., Huang, C., et al. (2016). Thicknesses of mare basalts on the Moon from gravity and topography. *Journal of Geophysical Research: Planets*, 121(5), 854–870. <https://doi.org/10.1002/2016JE005008>
- Greenhagen, B. T., Lucey, P. G., Wyatt, M. B., Glotch, T. D., Allen, C. C., Arnold, J. A., et al. (2010). Global silicate mineralogy of the moon from the Diviner Lunar Radiometer. *Science*, 329(5998), 1507–1509. <https://doi.org/10.1126/science.1192196>
- Grimm, R. E. (2013). Geophysical constraints on the lunar Procellarum KREEP Terrane. *Journal of Geophysical Research: Planets*, 118(4), 768–778. <https://doi.org/10.1029/2012je004114>
- Grimm, R. E. (2018). New analysis of the Apollo 17 surface electrical properties experiment. *Icarus*, 314, 389–399. <https://doi.org/10.1016/j.icarus.2018.06.007>
- Gross, J., Hilton, A., Prissel, T. C., Setera, J. B., Korotev, R. L., & Calzada-Diaz, A. (2020). Geochemistry and petrogenesis of Northwest Africa 10401: A new type of the Mg-suite rocks. *Journal of Geophysical Research: Planets*, 125(5), e2019JE006225. <https://doi.org/10.1029/2019je006225>
- Hagermann, A., & Tanaka, S. (2006). Ejecta deposit thickness, heat flow, and a critical ambiguity on the Moon. *Geophysical Research Letters*, 33(19), L19203. <https://doi.org/10.1029/2006GL027030>
- Hagerty, J. J., Shearer, C. K., & Vaniman, D. T. (2006). Heat-producing elements in the lunar mantle: Insights from ion microprobe analyses of lunar pyroclastic glasses. *Geochimica et Cosmochimica Acta*, 70(13), 3457–3476. <https://doi.org/10.1016/j.gca.2006.04.013>
- Hahn, B. C., McLennan, S. M., & Klein, E. C. (2011). Martian surface heat production and crustal heat flow from Mars Odyssey Gamma-Ray spectrometry. *Geophysical Research Letters*, 38(14), L14203. <https://doi.org/10.1029/2011GL047435>
- Haskin, L. A. (1998). The Imbrium impact event and the thorium distribution at the lunar highlands surface. *Journal of Geophysical Research*, 103(E1), 1679–1689. <https://doi.org/10.1029/97je03035>
- Haskin, L. A., Gillis, J. J., Korotev, R. L., & Jolliff, B. L. (2000). The materials of the lunar Procellarum KREEP Terrane: A synthesis of data from geomorphological mapping, remote sensing, and sample analyses. *Journal of Geophysical Research*, 105(E8), 20403–20415. <https://doi.org/10.1029/1999je001128>
- Hawke, B. R., Peterson, C. A., Blewett, D. T., Bussey, D. B. J., Lucey, P. G., Taylor, G. J., & Spudis, P. D. (2003). Distribution and modes of occurrence of lunar anorthosite. *Journal of Geophysical Research*, 108(E6), 5050. <https://doi.org/10.1029/2002je001890>
- Jarosewich, E. (2006). Chemical analyses of meteorites at the Smithsonian Institution: An update. *Meteoritics & Planetary Sciences*, 41(9), 1381–1382.
- Jaupart, C., & Mareschal, J. C. (2010). *Heat generation and transport in the Earth*. Cambridge University Press.
- Jaupart, C., & Mareschal, J.-C. (2014). 4.2: Constraints on crustal heat production from heat flow data. In H. D. Holland & K. K. Turekian (Eds.), *Treatise on geochemistry* (2nd ed., pp. 53–73). Elsevier. <https://doi.org/10.1016/B978-0-08-095975-7.00302-8>
- Jaupart, C., Mareschal, J. C., & Schubert, G. (2007). Heat flow and thermal structure of the lithosphere. *Treatise on geophysics*, 6, 217–252. <https://doi.org/10.1016/b978-0-44452748-6/00104-8>
- Jolliff, B. L., Gillis, J. J., Haskin, L. A., Korotev, R. L., & Wieczorek, M. A. (2000). Major lunar crustal terranes: Surface expressions and crust-mantle origins. *Journal of Geophysical Research*, 105(E2), 4197–4216. <https://doi.org/10.1029/1999je001103>
- Keith, J. E., Clark, R. S., & Bennett, L. J. (1974). Determination of natural and cosmic ray induced radionuclides in Apollo 17 lunar samples. In *Lunar and planetary science conference proceedings* (Vol. 5, pp. 2121–2138).
- Konopliv, A. S., Park, R. S., Yuan, D. N., Asmar, S. W., Watkins, M. M., Williams, J. G., et al. (2013). The JPL lunar gravity field to spherical harmonic degree 660 from the GRAIL primary mission. *Journal of Geophysical Research: Planets*, 118(7), 1415–1434. <https://doi.org/10.1002/jgre.20097>
- Korenaga, J. (2008). Urey ratio and the structure and evolution of Earth's mantle. *Reviews of Geophysics*, 46(2), RG2007. <https://doi.org/10.1029/2007rg000241>
- Korotev, R. L. (1987). Mixing levels, the Apennine Front soil component, and compositional trends in the Apollo 15 soils. *Journal of Geophysical Research*, 92(B4), E411–E431. <https://doi.org/10.1029/jb092ib04p0e411>
- Korotev, R. L. (2012). Lunar meteorites from Oman. *Meteoritics & Planetary Sciences*, 47(8), 1365–1402. <https://doi.org/10.1111/j.1945-5100.2012.01393.x>
- Korotev, R. L. (2017). Update (2012–2017) on lunar meteorites from Oman. *Meteoritics & Planetary Sciences*, 52(6), 1251–1256. <https://doi.org/10.1111/maps.12869>
- Korotev, R. L., & Irving, A. J. (2021). Lunar meteorites from northern Africa. *Meteoritics & Planetary Sciences*, 56(2), 206–240. <https://doi.org/10.1111/maps.13617>
- Korotev, R. L., & Kremser, D. T. (1992). Compositional variations in Apollo 17 soils and their relationship to the geology of the Taurus-Littrow site. In *Lunar and planetary science conference proceedings* (Vol. 22, pp. 275–301).
- Korotev, R. L., Zeigler, R. A., Righter, K., Harvey, R. P., Corrigan, C. M., & McCoy, T. C. (2014). ANSMET meteorites from the Moon. In *Thirty-five seasons of US Antarctic meteorites (1976–2010): A pictorial guide to the collection* (pp. 101–130). Wiley.
- Kruijer, T. S., & Kleine, T. (2017). Tungsten isotopes and the origin of the Moon. *Earth and Planetary Science Letters*, 475, 15–24.
- Laneuville, M., Taylor, J., & Wieczorek, M. A. (2018). Distribution of radioactive heat sources and thermal history of the Moon. *Journal of Geophysical Research: Planets*, 123(12), 3144–3166. <https://doi.org/10.1029/2018je005742>
- Laneuville, M., Wieczorek, M. A., Breuer, D., & Tosi, N. (2013). Asymmetric thermal evolution of the Moon. *Journal of Geophysical Research: Planets*, 118(7), 1435–1452. <https://doi.org/10.1002/jgre.20103>
- Langmuir, C. H., & Asimow, P. D. (2005). Effect of water on magma and crustal density: Highly fractionated lavas in the Lau Basin and other wet spreading centers. *Geochimica et Cosmochimica Acta*, 69(10), A149.
- Langseth, M. G., Keihm, S. J., & Peters, K. (1976). Revised lunar heat-flow values. In *Lunar and planetary science conference proceedings* (Vol. 7, pp. 3143–3171).
- Laul, J. C., Hill, D. W., & Schmitt, R. A. (1974). Chemical studies of Apollo 16 and 17 samples. In *Lunar and planetary science conference proceedings* (Vol. 5, pp. 1047–1066).

- Lawrence, D. J., Elphic, R. C., Feldman, W. C., Prettyman, T. H., Gasnault, O., & Maurice, S. (2003). Small-area thorium features on the lunar surface. *Journal of Geophysical Research*, *108*(E9), 5102. <https://doi.org/10.1029/2003je002050>
- Lawrence, D. J., Feldman, W. C., Barraclough, B. L., Binder, A. B., Elphic, R. C., Maurice, S., & Prettyman, T. H. (2000). Thorium abundances on the lunar surface. *Journal of Geophysical Research*, *105*(E8), 20307–20331.
- Lemelin, M., Lucey, P. G., Song, E., & Taylor, G. J. (2015). Lunar central peak mineralogy and iron content using the Kaguya Multiband Imager: Reassessment of the compositional structure of the lunar crust. *Journal of Geophysical Research: Planets*, *120*(5), 869–887. <https://doi.org/10.1002/2014je004778>
- Lognonné, P., Gagnepain-Beyneix, J., & Chenet, H. (2003). A new seismic model of the moon: Implications for structure, thermal evolution and formation of the moon. *Earth and Planetary Science Letters*, *211*(1–2), 27–44. [https://doi.org/10.1016/s0012-821x\(03\)00172-9](https://doi.org/10.1016/s0012-821x(03)00172-9)
- Lyubetskaya, T., & Korenaga, J. (2007). Chemical composition of Earth's primitive mantle and its variance: 1. Method and results. *Journal of Geophysical Research*, *112*(B3), B03211. <https://doi.org/10.1029/2005jb004223>
- Martinot, M., Besse, S., Flahaut, J., Quantin-Nataf, C., Lozac'h, L., & Van Westrenen, W. (2018). Mineralogical diversity and geology of Humboldt crater derived using Moon Mineralogy Mapper data. *Journal of Geophysical Research: Planets*, *123*(2), 612–629. <https://doi.org/10.1002/2017je005435>
- McCallum, I. S., & Schwartz, J. M. (2001). Lunar Mg suite: Thermobarometry and petrogenesis of parental magmas. *Journal of Geophysical Research*, *106*(E11), 27969–27983.
- McDonough, W. F., & Sun, S. S. (1995). The composition of the Earth. *Chemical Geology*, *120*(3–4), 223–253. [https://doi.org/10.1016/0009-2541\(94\)00140-4](https://doi.org/10.1016/0009-2541(94)00140-4)
- Meyer, C. (2005). Lunar Sample Compendium. NASA STI/Recon Technical Report No. 6 (p. 11039).
- Moriarty, D. P., Watkins, R. N., & Petro, N. E. (2020). Mineralogical diversity of the lunar south pole: Critical context for Artemis sample return goals and interpretation. In *Lunar surface science workshop* (Vol. 2241, p. 5152).
- Nagihara, S., Zacny, K., & Siegler, M., & the Honeybee Robotics LISTER Team. (2021). *Heat flow measurements planned for upcoming robotic lunar-landing missions, AGU Fall Meeting, Abstract P54C-04*.
- Neal, C. R., Banerdt, W. B., & Alkalai, L. (2010). LUNETTE: Establishing a lunar geophysical network without nuclear power through a discovery-class mission. In *41st Annual lunar and planetary science conference* (Vol. 1533, p. 2710).
- Neal, C. R., Weber, R. C., Banerdt, W. B., Beghein, C., Chi, P., Currie, D., et al. (2020). The Lunar Geophysical Network, Final Report NASA Planetary Mission Concepts Study NNH18ZDA001N-PMCS.
- Ngo, P., Nagihara, S., Sanigepalli, V., Sanasarian, L., & Zacny, K. (2019). Heat flow probe for short-duration lander missions under NASA's commercial lunar Payload Service Program. In *AGU Fall Meeting Abstracts, 2019, P33C-05*.
- Ohtake, M., Matsunaga, T., Haruyama, J., Yokota, Y., Morota, T., Honda, C., et al. (2009). The global distribution of pure anorthosite on the Moon. *Nature*, *461*(7261), 236–240. <https://doi.org/10.1038/nature08317>
- Pahlevan, K., & Stevenson, D. J. (2007). Equilibration in the aftermath of the lunar-forming giant impact. *Earth and Planetary Science Letters*, *262*(3–4), 438–449. <https://doi.org/10.1016/j.epsl.2007.07.055>
- Paige, D. A., Siegler, M. A., & Warren, P. (2016). New constraints on lunar heat flow rates from LRO diviner lunar radiometer experiment polar observations. In *47th lunar and planetary science conference #2753*.
- Plesa, A. C., Tosi, N., Grott, M., & Breuer, D. (2015). Thermal evolution and Urey ratio of Mars. *Journal of Geophysical Research: Planets*, *120*(5), 995–1010. <https://doi.org/10.1002/2014je004748>
- Prettyman, T. H. (2021). Lunar prospector GRS elemental Abundance Bundle. *NASA Planetary Data System*. <https://doi.org/10.17189/1519384>
- Prettyman, T. H., Hagerty, J. J., Elphic, R. C., Feldman, W. C., Lawrence, D. J., McKinney, G. W., & Vaniman, D. T. (2006). Elemental composition of the lunar surface: Analysis of gamma ray spectroscopy data from Lunar Prospector. *Journal of Geophysical Research*, *111*, E2656. <https://doi.org/10.1029/2005JE002656>
- Rhodes, J. M., Rodgers, K. V., Shih, C., Bansal, B. M., Nyquist, L. E., & Wiesmann, H. (1974). The relationship between geology and soil chemistry at the Apollo 17 landing site. *Lunar and Planetary Science Conference*, *5*, 630.
- Rose, H. J., Jr., Cuttitta, F., Berman, S., Brown, F. W., Carron, M. K., Christian, R. P., et al. (1974). Chemical composition of rocks and soils at Taurus-Littrow. In *Presented at the lunar and planetary science conference proceedings* (pp. 1119–1133).
- Rudnick, R. L., Gao, S., Holland, H. D., & Turekian, K. K. (2003). Composition of the continental crust. *The crust*, *3*, 1–64. [https://doi.org/10.1016/0016-7037\(95\)00038-2](https://doi.org/10.1016/0016-7037(95)00038-2)
- Ryder, G. R. A. H. A. M., & Wood, J. A. (1977). Serenitatis and Imbrium impact melts: Implications for large-scale layering in the lunar crust. In *Lunar and planetary science conference proceedings* (Vol. 8, pp. 655–668).
- Scholten, F., Oberst, J., Matz, K. D., Roatsch, T., Wählisch, M., Speyerer, E. J., & Robinson, M. S. (2012). GLD100: The near-global lunar 100 m raster DTM from LROC WAC stereo image data. *Journal of Geophysical Research*, *117*(E12). <https://doi.org/10.1029/2011je003926>
- Schubert, G., Stevenson, D., & Cassen, P. (1980). Whole planet cooling and the radiogenic heat source contents of the Earth and Moon. *Journal of Geophysical Research*, *85*(B5), 2531–2538. <https://doi.org/10.1029/JB085iB05p02531>
- Shearer, C. K., Elardo, S. M., Petro, N. E., Borg, L. E., & McCubbin, F. M. (2015). Origin of the lunar highlands Mg-suite: An integrated petrology, geochemistry, chronology, and remote sensing perspective. *American Mineralogist*, *100*(1), 294–325. <https://doi.org/10.2138/am-2015-4817>
- Siegler, M. A. (2022). Lunar heat flow: Global predictions and reduced heat flux (version 1). *Zenodo*. <https://doi.org/10.5281/ZENODO.6476036>
- Siegler, M. A., Miller, R. S., Keane, J. T., Laneuville, M., Paige, D. A., Matsuyama, I., et al. (2016). Lunar true polar wander inferred from polar hydrogen. *Nature*, *531*(7595), 480–484. <https://doi.org/10.1038/nature17166>
- Siegler, M. A., & Smrekar, S. E. (2014). Lunar heat flow: Regional prospective of the Apollo landing sites. *Journal of Geophysical Research: Planets*, *119*(1), 47–63. <https://doi.org/10.1002/2013JE004453>
- Spohn, T., & Breuer, D. (2002). Surface heat flow, radiogenic heating, and the evolution of the moon. In *Presented at the EGS General Assembly Conference Abstracts* (p. 6000).
- Spohn, T., Konrad, W., Breuer, D., & Ziethe, R. (2001). The longevity of lunar volcanism: Implications of thermal evolution calculations with 2D and 3D mantle convection models. *Icarus*, *149*(1), 54–65. <https://doi.org/10.1006/icar.2000.6514>
- Spudis, P. D., & Davis, P. A. (1986). A chemical and petrological model of the lunar crust and implications for lunar crustal origin. *Journal of Geophysical Research*, *91*(B13), E84–E90. <https://doi.org/10.1029/jb091i13p00e84>
- Stein, C. A. (1995). Heat flow of the Earth. In *Global Earth Physics: A Handbook of Physical Constants* (Vol. 1, pp. 144–158).
- Su, Y. J. (2003). Mid-ocean ridge basalt trace element systematics: Constraints from database management, ICPMS analysis, global data compilation, and petrologic modeling.

- Sun, C., Graff, M., & Liang, Y. (2017). Trace element partitioning between plagioclase and silicate melt: The importance of temperature and plagioclase composition, with implications for terrestrial and lunar magmatism. *Geochimica et Cosmochimica Acta*, 206, 273–295. <https://doi.org/10.1016/j.gca.2017.03.003>
- Taylor, G. J., & Wieczorek, M. A. (2014). Lunar bulk chemical composition: A post-gravity recovery and interior laboratory reassessment. *Philosophical Transactions of the Royal Society A: Mathematical, Physical & Engineering Sciences*, 372(2024), 20130242. <https://doi.org/10.1098/rsta.2013.0242>
- Taylor, S. R., & McLennan, S. M. (1985). The continental crust: Its composition and evolution.
- Taylor, S. R., Taylor, G. J., & Taylor, L. A. (2006). The Moon: A Taylor perspective. *Geochimica et Cosmochimica Acta*, 70(24), 5904–5918. <https://doi.org/10.1016/j.gca.2006.06.262>
- Thomson, B. J., Grosfils, E. B., Bussey, D. B. J., & Spudis, P. D. (2009). A new technique for estimating the thickness of mare basalts in Imbrium Basin. *Geophysical Research Letters*, 36(12), L12201. <https://doi.org/10.1029/2009GL037600>
- Waelenke, H., Palme, H., Baddenhausen, H., Dreibus, G., Jagoutz, E., Kruse, H., et al. (1974). Chemistry of Apollo 16 and 17 samples—Bulk composition, late stage accumulation and early differentiation of the moon. In *Presented at the lunar and planetary science conference proceedings* (pp. 1307–1335).
- Waelenke, H., Palme, H., Baddenhausen, H., Dreibus, G., Jagoutz, E., Kruse, H., et al. (1975). New data on the chemistry of lunar samples: Primary matter in the lunar highlands and the bulk composition of the moon. In *Presented at the lunar and planetary science conference proceedings* (pp. 1313–1340).
- Wagner, R. V., Robinson, M. S., Speyerer, E. J., & Plescia, J. B. (2014). Locations of Anthropogenic sites on the moon. In *Lunar and planetary science conference* (Vol. 2259).
- Warren, P. H. (2001). Compositional structure within the lunar crust as constrained by Lunar Prospector thorium data. *Geophysical Research Letters*, 28(13), 2565–2568. <https://doi.org/10.1029/2000gl012739>
- Warren, P. H. (2005). “New” lunar meteorites: Implications for composition of the global lunar surface, lunar crust, and the bulk Moon. *Meteoritics & Planetary Sciences*, 40(3), 477–506. <https://doi.org/10.1111/j.1945-5100.2005.tb00395.x>
- Warren, P. H. (2011). Stable-isotopic anomalies and the accretionary assemblage of the Earth and Mars: A subordinate role for carbonaceous chondrites. *Earth and Planetary Science Letters*, 311(1–2), 93–100. <https://doi.org/10.1016/j.epsl.2011.08.047>
- Warren, P. H., & Kallemeyn, G. W. (1991). The MacAlpine Hills lunar meteorite and implications of the lunar meteorites collectively for the composition and origin of the Moon. *Geochimica et Cosmochimica Acta, The Macalpine Hills Lunar Meteorite Consortium*, 55(11), 3123–3138. [https://doi.org/10.1016/0016-7037\(91\)90477-M](https://doi.org/10.1016/0016-7037(91)90477-M)
- Warren, P. H., & Rasmussen, K. L. (1987). Megaregolith insulation, internal temperatures, and bulk uranium content of the moon. *Journal of Geophysical Research*, 92(B5), 3453–3465. <https://doi.org/10.1029/JB092iB05p03453>
- Warren, P. H., & Wasson, J. T. (1979). The origin of KREEP. *Reviews of Geophysics*, 17(1), 73–88. <https://doi.org/10.1029/rg017i001p00073>
- Wasson, J. T., & Kallemeyn, G. W. (1988). Compositions of chondrites. *Philosophical Transactions of the Royal Society of London: Series A: Mathematical and Physical Sciences*, 325(1587), 535–544.
- Weber, R. C., Lin, P. Y., Garner, E. J., Williams, Q., & Lognonné, P. (2011). Seismic detection of the lunar core. *Science*, 331(6015), 309–312. <https://doi.org/10.1126/science.1199375>
- Wieczorek, M. (2012). GRAIL crustal thickness Archive. *Zenodo*. <https://doi.org/10.5281/zenodo.997347>
- Wieczorek, M. A. (2018). Strength, depth, and geometry of magnetic sources in the crust of the Moon from localized power spectrum analysis. *Journal of Geophysical Research: Planets*, 123(1), 291–316.
- Wieczorek, M. A., Neumann, G. A., Nimmo, F., Kiefer, W. S., Taylor, G. J., Melosh, H. J., et al. (2013). The crust of the moon as seen by GRAIL. *Science*, 339(6120), 671–675. <https://doi.org/10.1126/science.1231530>
- Wieczorek, M. A., & Phillips, R. J. (2000). The “Procellarum KREEP Terrane”: Implications for mare volcanism and lunar evolution. *Journal of Geophysical Research*, 105(E8), 20417–20430. <https://doi.org/10.1029/1999JE001092>
- Wieczorek, M. A., & Zuber, M. T. (2001). The composition and origin of the lunar crust: Constraints from central peaks and crustal thickness modeling. *Geophysical Research Letters*, 28(21), 4023–4026. <https://doi.org/10.1029/2001gl012918>
- Williams, J. P., Paige, D. A., Greenhagen, B. T., & Sefton-Nash, E. (2017). The global surface temperatures of the moon as measured by the Diviner lunar radiometer experiment. *Icarus*, 283, 300–325. <https://doi.org/10.1016/j.icarus.2016.08.012>
- Wilson, J. T., Eke, V. R., Massey, R. J., Elphic, R. C., Jolliff, B. L., Lawrence, D. J., et al. (2015). Evidence for explosive silicic volcanism on the Moon from the extended distribution of thorium near the Compton-Belkovich Volcanic Complex. *Journal of Geophysical Research: Planets*, 120(1), 92–108. <https://doi.org/10.1002/2014je004719>
- Workman, R. K., & Hart, S. R. (2005). Major and trace element composition of the depleted MORB mantle (DMM). *Earth and Planetary Science Letters*, 231(1–2), 53–72. <https://doi.org/10.1016/j.epsl.2004.12.005>
- Yamamoto, S., Nakamura, R., Matsunaga, T., Ogawa, Y., Ishihara, Y., Morota, T., et al. (2012). Massive layer of pure anorthosite on the Moon. *Geophysical Research Letters*, 39(13), L13201. <https://doi.org/10.1029/2012gl052098>
- Yamashita, N., Hasebe, N., Reedy, R. C., Kobayashi, S., Karouji, Y., Hareyama, M., et al. (2010). Uranium on the moon: Global distribution and U/Th ratio. *Geophysical Research Letters*, 37, L10201. <https://doi.org/10.1029/2010GL043061>
- Yoshida, S., Tanaka, S., Hagermann, A., Hayakawa, M., Fujimura, A., & Mizutani, H. (2001). Derivation of globally Averaged lunar heat flow from the local heat flow values and the thorium distribution at the surface: Expected Improvement by the LUNAR-A mission. In *Lunar and planetary science conference* (Vol. 1571).
- Zhang, D., Li, X., Li, Q., Lang, L., & Zheng, Y. (2014). Lunar surface heat flow mapping from radioactive elements measured by Lunar Prospector. *Acta Astronautica*, 99, 85–91. <https://doi.org/10.1016/j.actaastro.2014.01.020>
- Zuber, M. T., Smith, D. E., Lehman, D. H., Hoffman, T. L., Asmar, S. W., & Watkins, M. M. (2012). Gravity Recovery and Interior Laboratory (GRAIL): Mapping the lunar interior from crust to core. In *GRAIL: Mapping the Moon's interior* (pp. 3–24). Springer.
- Zuo, W., Li, C., & Zhang, Z. (2014). Scientific data and their release of Chang’E-1 and Chang’E-2. *Chinese Journal of Geochemistry*, 33(1), 24–44. <https://doi.org/10.1007/s11631-014-0657-3>